Published in final edited form as:
Biochemistry. 2007 March 13; 46(10): 2608–2621. doi:10.1021/bi061381h.

Stereochemistry Modulates Stability of Reduced Inter-Strand Cross-Links Arising From *R*- and *S*-α-CH_3-γ-OH-1,N^2-propano-2′-Deoxyguanosine in the 5′-CpG-3′ DNA Sequence

Young-Jin Cho, **Ivan D. Kozekov**, **Thomas M. Harris**, **Carmelo J. Rizzo**, and **Michael P. Stone** [

Department of Chemistry, Center in Molecular Toxicology, Vanderbilt-Ingram Cancer Center, Vanderbilt University, Nashville, Tennessee 37235

Abstract

The solution structures of 5′-Cp-N^2-dG-3′-*R*-(α)-CH_3-propyl-5′-Cp-N^2-dG-3′ and 5′-Cp-N^2-dG-3′-*S*-(α)-CH_3-propyl-5′-Cp-N^2-dG-3′ inter-strand DNA cross-links in the 5′-CpG-3′ sequence were determined by NMR spectroscopy. These were utilized as chemically stable surrogates for the corresponding carbinolamine inter-strand cross-links arising from the crotonaldehyde and acetaldehyde-derived *R*- and *S*-α-CH_3-γ-OH-1,N^2-propanodeoxyguanosine adducts. The results provide an explanation for the observation that inter-strand cross-link formation in the 5′-CpG-3′ sequence by the *R*- and *S*-α-CH_3-γ-OH-1,N^2-propanodeoxyguanosine adducts is dependent upon stereochemistry, favoring the *R*-α-CH_3-γ-OH-1,N^2-propanodeoxyguanosine adduct [Kozekov, I.D., Nechev, L.V., Moseley, M.S., Harris, C.M., Rizzo, C.J., Stone, M.P., & Harris, T.M. (2003) *J. Am. Chem. Soc. 125*, 50–61]. Molecular dynamics calculations, restrained by NOE-based distances and empirical restraints, revealed that both the 5′-Cp-N^2-dG-3′-*R*-(α)-CH_3-propyl-5′-Cp-N^2-dG-3′ and 5′-Cp-N^2-dG-3′- *S*-(α)-CH_3-propyl-5′-Cp-N^2-dG-3′ cross-links were located in the minor groove and retained Watson-Crick hydrogen bonds at the tandem cross-linked C•G base pairs. However, for the 5′-Cp-N^2-dG-3′- *R*-(α)-CH_3-propyl-5′-Cp-N^2-dG-3′ cross-link, the (α)-CH_3 group was positioned in the center of the minor groove, whereas for the 5′-Cp-N^2-dG-3′- *S*-(α)-CH_3-propyl-5′-Cp-N^2-dG-3′ cross-link, the (α)-CH_3 group was positioned in the 3′ direction, showing steric interference with the DNA helix. The 5′-Cp-N^2-dG-3′-*S*-(α)-CH_3-propyl-5′-Cp-N^2-dG-3′ cross-link showed lower thermal stability as evidenced by NMR spectroscopy as a function of temperature. The two cross-links also exhibited apparent differences in the conformation of the inter-strand three-carbon cross-link, which may also contribute to the lower apparent thermodynamic stability of the 5′-Cp-N^2-dG-3′- *S*-(α)-CH_3-propyl-5′-Cp-N^2-dG-3′ cross-link.

Crotonaldehyde **1**, an α,β-unsaturated aldehyde, is genotoxic and mutagenic in human lymphoblasts (1). It induces liver tumors in rodents (2). Michael addition of deoxyguanosine to crotonaldehyde yields the diastereomeric *R*- and *S*-α-CH_3-γ-OH-1,N^2-propano-2′-deoxyguanosine adducts **2a** and **2b** (Chart 1) (3–6). A second DNA adduction pathway yields

[Author to whom correspondence should be addressed. Telephone 615-322-2589; FAX 615-322-7591; email michael.p.stone@vanderbilt.edu.

[1]Abbreviations: DQF-COSY, double-quantum filtered correlation spectroscopy; HMBC, heteronuclear multiple bond correlation spectroscopy; MALDI-TOF, matrix assisted laser desorption ionization time-of-flight mass spectrometry; NOE, nuclear Overhauser enhancement; NOESY, nuclear Overhauser enhancement spectroscopy; R_1^x, sixth root residual; rMD, restrained molecular dynamics; rmsd, root mean square deviation; TOCSY, total correlation spectroscopy; TPPI, time-proportional phase increment.

[2]The definitions of the prochiral protons at the enantiotopic protons at C_β and C_γ of the cross-link are based upon the Cahn, Ingold, and Prelog nomenclature. The proton $H_{\gamma 1}$ is the pro-*S* proton at C_γ, $H_{\gamma 2}$ is the pro-*R* proton at C_γ, $H_{\beta 1}$ is the pro-*R* proton at C_β and $H_{\beta 2}$ is the pro-*S* proton at C_β.

paraldol-releasing DNA adducts (7), primarily N^2-(3-hydroxybutylidene)-dG (8). Adducts **2a** and **2b** also form through the reaction of acetaldehyde, a mutagen and potential human carcinogen (9), with deoxyguanosine (6,10). The *R*- and *S*-α-CH_3-γ-OH-PdG adducts **2a** and **2b** have been detected in human and rodent tissues (11–13). In humans, these probably result from various endogenous and exogenous exposures, including lipid peroxidation (11,14,15), exposure to tobacco smoke (16,17), and exposure to N-nitrosopyrrolidine (18,19).

The site-specific synthesis of oligodeoxynucleotides containing cyclic adducts **2a** or **2b** (20–22) enabled their chemistry to be examined in duplex DNA. When adducts **2a** or **2b** were placed into oligodeoxynucleotide duplexes at 5′-CpG-3′ sequences, Kozekov et al. (23) trapped inter-strand saturated three carbon cross-links by treatment with $NaCNBH_3$, corroborating the reports of Wang et al. (6,8). Significantly, cross-linking efficiency was dependent upon the stereochemistry of the adduct, favoring the *R*-α-CH_3-γ-OH-PdG adduct **2a**, as opposed to the *S*-α-CH_3-γ-OH-PdG adduct **2b**. However, both the *R*-α-CH_3-γ-OH-PdG adduct **2a**, and the *S*-α-CH_3-γ-OH-PdG adduct **2b** readily formed N-terminal conjugates with the peptide KWKK (24). This implied that both the adducts **2a** and **2b** underwent opening to the corresponding aldehydes **3a** or **3b** when placed opposite dC in duplex DNA, but only aldehyde **3a** efficiently formed inter-strand cross-links in the 5′-CpG-3′ sequence.

A series of stable-isotope-edited NMR experiments showed that crotonaldehyde-derived adduct **2a** yielded carbinolamine cross-link **5a**, with the corresponding imine **6a** and pyrimidopurinone **7a** cross-links remaining below the level of detection at equilibrium in duplex DNA (25). Molecular modeling suggested a thermodynamic basis for this observation: the inter-strand cross-link arising from the N^2-(*R*-α-CH_3-γ-OH-1,N^2-propano-2′)-dG adduct **2a** introduced less disruption into the duplex than did that arising from the N^2-(*S*-α-CH_3-γ-OH-1,N^2-propano-2′)-dG adduct **2b**, due to differing orientations of the *R*- and *S*-CH_3 groups (25).

Herein, solution structures of stereoisomeric reduced 5′-Cp-N^2-d<u>G</u>-3′- *R*-(α)-CH_3-propyl-5′-Cp-N^2-d<u>G</u>-3′ and 5′-Cp-N^2-d<u>G</u>-3′-*S*-(α)-CH_3-propyl-5′-Cp-N^2-d<u>G</u>-3′ inter-strand DNA cross-links **8a** and **8b** in the 5′-CpG-3′ sequence (Chart 2) are determined by NMR spectroscopy. These are utilized as chemically stable surrogates for the carbinolamine inter-strand cross-links **5a** and **5b** arising from the crotonaldehyde and acetaldehyde-derived *R*- and *S*-α-CH_3-γ-OH-1,N^2-propanodeoxyguanosine adducts. A similar strategy was employed by Liu et al. (26) to examine replication-coupled repair of these crotonaldehyde and acetaldehyde-derived inter-strand cross-links. The present structural data explains the observation that inter-strand cross-link formation in the 5′-CpG-3′ sequence favors the N^2-(*R*-α-CH_3-γ-OH-1,N^2-propano-2′)-dG adduct **2a** (23). Molecular dynamics calculations, restrained by NOE-based distances and empirical restraints, reveal that both cross-links **8a** and **8b** are located in the minor groove and retain Watson-Crick hydrogen bonds at the tandem cross-linked C•G base pairs. However, for cross-link **8a**, the (α)-CH_3 group is positioned in the center of the minor groove, whereas for cross-link **8b**, the (α)-CH_3 group interferes sterically with the DNA helix. Cross-link **8b** shows lower thermal stability as evidenced by NMR spectroscopy as a function of temperature. The two cross-links also exhibit differences in the conformation of the inter-strand three-carbon cross-link, which may contribute to the lower thermodynamic stability of cross-link **8b**.

MATERIALS AND METHODS

Oligodeoxynucleotide Synthesis

Oligodeoxynucleotides containing site-specific γ-OH-PdG and α-CH_3-γ-OH-PdG adducts were prepared as previously described (20–22). All commercially obtained chemicals were used as received. Concentrations of the single-stranded oligodeoxynucleotides were

determined from calculated extinction coefficients at 260 nm (27). The concentrations of the single stranded oligodeoxynucleotides were determined from extinction coefficients of 11.3 × 10^4 cm^{-1} and 11.1 × 10^4 cm^{-1}, respectively, at 260 nm.

HPLC

Oligodeoxynucleotide purification and analysis of enzymatic digestions were performed on a Beckman HPLC system (32 Karat software version 3.1, pump module 125) with a diode array UV detector (module 168) monitoring at 260 nm using a Waters YMC ODS-AQ column (250 mm × 4.6 mm i.d., 1.5 mL/min for analysis and 250 mm × 10 mm i.d., 5 mL/min for purification). The mobile phase was CH_3CN in 0.1 M, pH 7.0 $NH_4{}^+COO^-$. Gradient 1 was 1 to 10% CH_3CN, linear gradient over 15 min; 10–20% linear gradient over 5 min; 20%, isocratic for 5 min; 20 to 100%, linear gradient over 3 min; 100%, isocratic for 2 min; 100 to 1%, linear gradient over 3 min. Gradient 2 was 1 to 5% CH_3CN linear gradient over 5 min; 5 - 9.5% linear gradient over 15 min; 9.5 - 100% linear gradient over 3 min; 100% isocratic for 2 min; 100 to 1% linear gradient over 3 min.

Capillary Gel Electrophoresis

Electrophoretic analyses were carried out using a Beckman P/ACE MDQ instrument system (32 Karat software, version 5.0) monitored at 260 nm on a 31.2 cm × 100 μm eCAP capillary with samples applied at 10 kV and run at 9 kV. The capillary was packed with the manufacturer's 100-R gel (for ss-DNA) using a Tris-borate buffer system containing 7 M urea.

Mass Spectrometry

MALDI-TOF mass spectra (negative ion) of modified oligodeoxynucleotides were obtained on a Voyager Elite DE instrument (Perseptive Biosystems) at the Vanderbilt Mass Spectrometry Facility using a 3-hydroxypicolinic acid matrix containing ammonium hydrogen citrate (7 mg/mL) to suppress multiple sodium and potassium adducts.

Enzymatic Digestions

Enzymatic digestion was carried out in one step. The oligodeoxynucleotides (0.2–0.5 A_{260} units) were dissolved in 30 μL of buffer containing 10 mM Tris-HCl, and 10 mM $MgCl_2$ (pH 7.0), and incubated with DNase I (8 units, Promega), snake venom phosphodiesterase I (0.02 units, Sigma), and alkaline phosphatase (1.7 units, *E. coli*; Sigma) at 37 °C for 90 min. The mixture was analyzed by reversed phase HPLC as described above. Adducted deoxynucleosides were identified by comparison with authentic samples based on retention times, co-injection, and UV spectra.

Melting Studies

0.5 A_{260} unit of cross-linked duplex was dissolved in 0.5 mL of buffer containing 10 mM Na_2HPO_4/NaH_2PO_4, 0.1 M NaCl, 50 μM Na_2EDTA (pH 7.0). The UV absorbance at 260 nm was monitored at 1 min intervals with a 1 °C/min temperature gradient. The temperature was cycled between 5 and 95 °C. The first derivative of the melting curve was used to establish the T_m values.

N^2-(S-3-Aminobutyl)-2′-deoxyguanosine and N^2-(S-3-Amino-1-methylpropyl-)2′-deoxyguanosine

(*S*)-1,3-Diaminobutane dihydrochloride (30 mg, 0.187 mmol) (28) was added to a solution of O^6-(2-trimethylsilylethyl)-2-fluoro-2′-deoxyinosine (10 mg, 0.027 mmol), DMSO (200 μL), and diisopropylethylamine (100 μL). The mixture was stirred at 65 °C for 24 h. The volatiles were removed *in vacuo* with a centrifugal evaporator. The residue was dissolved in 5% acetic

acid (500 μL) and stirred for 2 h at room temperature to remove the O^6-protecting group. The mixture was neutralized with 1 M NaOH and purified by HPLC (Gradient 1) to give an 85% combined yield of products. N^2-(*S*-3-amino-butyl)-2′-deoxyguanosine (7.1 mg); ^{1}H NMR (DMSO-d_6) δppm 7.88 (s, 1H, H8), 6.15 (t, J = 7.0 Hz, 1H, H1′), 4.36 (m, 1H, H3′), 3.80 (m, 1H, H4′), 3.56 (m, 1H, H5′), 3.49 (m, 1H, H5″), 3.34 (m, 2H, NH-C$\underline{H}_2$), 3.12 (m, 1H, CH-NH_2), 2.60 (m, 1H, H2′), 2.20 (m, 1H, H2″), 1.73 (m, 1H, C$\underline{H}_2$-CH), 1.65 (m, 1H, C$\underline{H}_2$-CH), 1.15 (d, J = 7.0 Hz, 3H, CH_3), N1H and OH signals not observed; and N^2-(*S*-3-amino-1-methylpropyl)-2′-deoxyguanosine (acetate salt, 0.60 mg); ^{1}NMR (DMSO d_6): δ(ppm) 7.87 (s, 1H, H8), 6.13 (dd, 1H, H1′, $J_{1=}$ J_2 = 6.4 Hz), 4.35 (m, 1H, H3′), 4.00 (m, 1H, CH-CH_3), 3.80 (m, 1H, H4′), 3.55 (dd, 1H, H5′, $J_{1=}$ 5.2 Hz, $J_{2=}$ 11.5 Hz), 3.48 (dd, 1H, H5″, $J_{1=}$ 5.2 Hz, $J_{2=}$ 11.7 Hz), 2.65 (m, 2H, CH_2-NH_2), 2.60 (m, 1H, H2′), 2.20 (m, 1H, H2″), 1.80 (s, 3H, CH_3COO), 1.60 (q, 2H, CH-CH_2, J= 6.9 Hz), 1.15 (d, 3H, CH_3, J= 6.1 Hz), N^{1}H and OH signals not observed.

N^2-(R or S)-3-Amino-1-methylpropyl-dG Adducted Oligodeoxynucleotide

Oligodeoxynucleotides (120 A_{260} units) containing (6*S* or 6*R*)-8-hydroxy-6-methyl-5,6,7,8-tetrahydropyrimido[1,2-*a*]purin-10(3*H*)-one) (21) in 100 μL potassium phosphate buffer pH 7.0 and 100 μL ammonium hydroxide were incubated at room temperature for 24 h and then treated with $NaBH_4$ (1.0 mg, 27.5 μmol) and stirred at room temperature for an additional 2 h. The reactions were quenched with 5% acetic acid (500 μL) and the products isolated by HPLC. For the N^2-(*R*)-3-amino-1-methylpropyl-dG adducted oligodeoxynucleotide, 66 A_{260} units were purified by HPLC (Gradient 1). MALDI-TOF mass spectral analysis: calcd for [M - H]$^-$ 3715.7, found 3715.6. For the N^2-(*S*)-3-amino-1-methylpropyl-dG adducted oligodeoxynucleotide, 72 A_{260} units were purified. MALDI-TOF mass spectral analysis, calcd for [M - H]$^-$ 3715.7, found 3715.5.

Synthesis of Cross-linked Oligodeoxynucleotide Duplexes

The N^2-(*R* or *S*)-3-amino-1-methylpropyl-dG adducted oligodeoxynucleotide and its complement containing O^6-(2-timethylsilylethyl)-2-fluoro-2′- deoxyinosine were mixed in a plastic test tube with 300 μL 0.05 M sodium borate buffer (pH 9). The mixture was stirred at 45–47 °C and the reaction was monitored by HPLC and CGE. The reaction times were 2 days for the (*R*)-isomer and 5 days for the (*S*)-isomer. After the reaction was complete 5% acetic acid (500 μL) was added and the mixture was stirred for 1 h at room temperature. The cross-linked oligodeoxynucleotides were purified by HPLC and desalted on Sephadex G-25. For the 5′-Cp-N^2-d$\underline{G}$-3′-*R*-(α)-CH_3-propyl-5′-Cp-N^2-d$\underline{G}$-3′ crosslink **8a**, 62 A_{260} units were purified by HPLC. MALDI-TOF mass spectrometry: calcd for [M - H]$^-$ 7346.6, found 7349.4. For the 5′- Cp-N^2-d$\underline{G}$-3′- *S*-(α)-CH_3-propyl-5′-Cp-N^2-d$\underline{G}$-3′ crosslink **8b**, 52 A_{260} units were purified by HPLC (Gradient 2). MALDI-TOF mass spectrometry: calcd for [M - H]$^-$ 7346.6, found 7345.1.

NMR

Experiments were carried out at ^{1}H frequencies of at 500.13 MHz, 600.13, or 800.19 MHz. The duplex oligodeoxynucleotides were prepared at a concentration of 2 mM in 0.25 mL of 99.996% D_2O. The samples contained 10 mM NaH_2PO_4, 0.1 M NaCl, and 50 μM Na_2EDTA (pH 7.0). The samples were placed into micro-NMR tubes (Shigemi Glass, Inc., Allison Park, PA). ^{1}H NOESY experiments in D_2O were conducted at 30 °C. For each t_1 increment, 32 scans were averaged with pre-saturation of the HDO resonance. To derive distance restraints, spectra were recorded consecutively using TPPI phase cycling with mixing times of 60, 150, 250 and 350 ms. These were recorded with 2048 complex points in the acquisition dimension and 1024 real data points in the indirect dimension covering 9615.385 Hz. The relaxation delay was 2 s. The data in the d_2 dimension were zero-filled to give a matrix of 2K × 2K real points. NOESY

spectra for observation of exchangeable protons were recorded at 13 °C, in 9:1 H_2O:D_2O, using a field gradient Watergate pulse sequence (29) for water suppression. The spectra, consisting of 128 transients, were obtained with a cryogenic probe using States-TPPI phase cycling with mixing times of 200 and 250 ms. A squared sine-bell with 72° shift apodization was applied in d_1 dimension while cosine-squared bell apodization was applied in d_2 dimension. A total of 1536 real data points in the d_1 dimension and 512 points in d_2 dimension were acquired. Double quantum-filtered ^{1}H correlation (DQF-COSY) spectra (30,31) were collected at 30 °C with 2048 complex points in the acquisition dimension and 512 points in the d_2 dimension covering 6009.615 Hz and zero-filled to 1024 points to give a matrix of 1024 × 2048 real points. For each d_1 increment, 64 or 84 transients were averaged with pre-saturation of the HDO resonance. A squared sine-bell apodization function was applied in both dimensions. Chemical shifts of proton resonances were referenced to water. NMR data were processed on Silicon Graphics Octane workstations using NMRPipe (32) and assigned using FELIX2000 (Accelrys, Inc., San Diego, CA).

Experimental Distance Restraints

Footprints were drawn around cross-peaks for the NOESY spectrum measured at a mixing time of 250 ms to define the size and shape of individual crosspeaks, using the program FELIX2000. Identical footprints were transferred and fit to the crosspeaks obtained at the other two mixing times. Crosspeak intensities were determined by volume integration of the areas under the footprints. The intensities were combined with intensities generated from complete relaxation matrix analysis of a starting DNA structure to generate a hybrid intensity matrix (33). The program MARDIGRAS (v. 5.2) (34,35) was used to refine the hybrid matrix by iteration to optimize the agreement between the calculated and the experimental NOE intensities. The molecular motion was assumed to be isotropic. The noise level was set at the intensity of the weakest cross peak. Calculations were performed using the DNA starting models generated using the program INSIGHT II (Accelyris, Inc.), and NOE intensities derived from experiments at three mixing times, and with three τ_c values (2, 3, and 4 ns), yielding 18 sets of distances. Analysis of these data yielded the experimental distance restraints and standard deviations for the distance restraints used in subsequent restrained molecular dynamics calculations. For partially overlapped crosspeaks, the upper bounds on the distances were increased.

Restrained Molecular Dynamics

Calculations were performed on Silicon Graphics Octane workstations using the program AMBER 8.0 (36). Classical A-DNA and B-DNA structures were used as reference structures to create starting structures for potential energy minimization (37). The reduced cross-links were constructed between X^7 and Y^{19} using the BUILDER module of INSIGHT II (Accelrys, Inc., San Diego, CA). The program ANTECHAMBER was used and the atom types were based on AMBER atom types for parameterization. RESP atomic charges were calculated using GAUSSIAN98 (38) and the Hartree-Fock 6-31G* basis set. Initially constructed A and B-DNA starting structures were energy-minimized by the conjugate gradients method for 250 iterations using the AMBER 8.0 force field to relieve poor van der Walls contacts. This energy minimization used a constant dielectric without experimental restraints. The restraint energy function included terms describing distance restraints as square-well potentials. The generalized Born solvent model was used for rMD simulated annealing calculations with 0.1 M salt concentration, and the SHAKE algorithm was used (39,40). The van der Waals energy term used the Lennard-Jones potential energy function. The electrostatic term used the Coulomb function, based on a full set of partial charges (−1 per residue) and a distance-dependent dielectric constant of 4*r*. The nonbonded pair list was updated if any atom moved more than 0.5 Å, and the cutoff radius for nonbonded interactions was 15 Å. The effective energy function included terms describing distance restraints, in the form of square-well

potentials. The partial charges assigned to the adduct by RESP protocol are shown in Figure S2 of the Supporting Information.

Calculations were initiated by coupling to a heating bath, with a target temperature of 600 K. The force constants were 50 kcal mol^{-1} $Å^{-2}$ for empirical hydrogen bonding and class 1NOE restraints, 45, 40, 35, and 30 for class2, class3, class4, and class5 respectively. Those force constants were increased up 1.5 times during first 3ps heating, and reduced back to original values during the rest of calculations. The target temperature was reached and maintained for 5 ps. The molecules were cooled to 100 K over 12 ps for equilibrium dynamics. During the final 8 ps the temperature was reduced to 0 K. Coordinate sets were archived every 0.2 ps, and 10 structures from the last 5 ps were averaged in total. An average structure was subjected to 500 iterations of conjugate gradient energy minimization to obtain the final structure. Back-calculation of theoretical NMR intensities from the emergent structures was performed using the program CORMA (v. 5.2) (33). Helicoidal parameters were examined using the program 3DNA (41).

RESULTS

Synthesis of Inter-Strand Cross-Links 8a and 8b Arising From R- and S-α-CH_3-γ-OH-1,N^2-propano-2′-Deoxyguanosine Adducts in the 5′-CpG-3′ DNA Sequence

Dooley et al. (42) synthesized trimethylene inter-strand cross-links of the type N^2-dG-$(CH_2)_3$-N^2-dG using a post-oligomerization approach (Scheme 1). This involved the incorporation of O^6-protected 2-flourohypoxanthine into an oligodeoxynucleotide and its complement at the desired sites for cross-link formation. 1,3-Diaminopropane was reacted with one of the oligodeoxynucleotides giving the N^2-(3-aminopropyl)-dG adducted oligodeoxynucleotide. After purification this oligodeoxynucleotide was reacted with its complementary strand containing an O^6-protected 2-flourohypoxanthine to give the cross-linked oligodeoxynucleotide. To prepare the reduced crotonaldehyde cross-links using this strategy, (*R*)- and (*S*)-1,3-diaminobutane were required (28) This diamine is unsymmetrical, thus it was critical that the initial adduction reaction with the diamine proceed with high regioselectivity. Lao and Hecht reported the application of this strategy (10). We found that the nucleophilic aromatic substitution reaction of (*R*)-1,3-diaminobutane with excess O^6-(2-trimethylsilyl)-2-fluoroinosine nucleoside gave a 92:8 regiochemical mixture of products (Scheme 1). Consequently, an alternative strategy that would not give such a product mixture was pursued, starting with the stereochemically pure oligodeoxynucleotides containing crotonaldehyde adducts **2a** or **2b** (Scheme 2) (25). Reductive amination with ammonia and $NaBH_4$ gave the desired N^2-[3-amino-(1*R)*-methylpropyl]-adducted oligodeoxynucleotides. Condensation with a complementary oligodeoxynucleotide containing 2-fluorohypoxanthine gave the stereo- and regio-chemically pure cross-linked oligodeoxynucleotides **8a** and **8b**, which were characterized by mass spectrometry, and enzymatic digestion.

Thermal Stability of Inter-strand Cross-Links 8a and 8b Arising From R- and S-α-CH_3-γ-OH-1, N^2-propano-2′-Deoxyguanosine Adducts in the 5′-CpG-3′ Sequence

UV melting studies revealed that the oligodeoxynucleotide containing cross-link **8a** exhibited a higher T_m than did the oligodeoxynucleotide containing cross-link **8b**. Figure 1 shows the imino proton region of the NMR spectra for the two oligodeoxynucleotides containing cross-links **8a** and **8b**, respectively, in the 5′- CpG-3′ sequence, as a function of temperature. For both oligodeoxynucleotides, the N3 imino resonances for T^3, T^{10}, T^{17}, and T^{21} broadened and disappeared at temperatures above 50 °C, whereas the N1 imino resonances for X^7 and Y^{19} were observed at higher temperatures, consistent with the location of the cross-link between these bases. For the cross-link **8a** with *R* stereochemistry, the X^7 and Y^{19} imino resonances remained observable at 73° C (Figure 1A). In contrast, for the cross-link **8b** with *S*

stereochemistry, the X^7 and Y^{19} imino proton resonances broadened and disappeared at this temperature (Figure 1B).

Assignments of Non-exchangeable DNA Protons

(a) 5′-Cp-N^2-dG-3′-R-(α)-CH$_3$-propyl-5′-Cp-N^2-dG-3′ Cross-linked Adduct 8a—As shown in Figure 2 A,B, the complete sequential connectivity between the aromatic and the anomeric protons for both strands was accomplished (43, 44). An overlap occurred for the C^6 and X^7 H1′ resonances. The completion of the NOESY walk was indicative of a stable and ordered DNA conformation. These assignments were expanded into other regions of the spectrum to yield complete ^{1}H assignments for the H2′, H2″, H3′, and H4′ protons. The assignments of Y^{19} H2′ and H2″ were reversed compared to other deoxyriboses. Table S1 in the Supporting Information details the assignments of the non-exchangeable protons.

(b) *5′-Cp*-N^2-*dG-3′*-S-(α)-*CH$_3$-propyl-5′-Cp*-N^2-*dG-3′* Cross -linked Adduct 8b—As shown in Figure 2 C,D, the complete sequential connectivity between the aromatic and the anomeric protons for both strands was accomplished (43, 44). The chemical shifts for X^7 H1′, A^8 H1′, C^{18} H1′, and Y^{19} H1′ differed from those observed in the cross-link having *R*-(α)-CH_3 stereochemistry. Separate resonances were observed for C^6 H1′ at 5.49 ppm and X^7 H1′ at 5.78 ppm, respectively. The completion of NOESY walk was indicative of a stable and ordered DNA conformation. These assignments were expanded into other regions of ^{1}H NOESY spectrum to yield complete ^{1}H assignments for the H2′, H2″, H3′, and H4′ protons. The assignments of Y^{19} H2′ and H2″ were reversed as compared to other deoxyriboses. Table S1 in the Supporting Information details the assignments of the non-exchangeable protons.

Assignments of Exchangeable DNA Protons

(a) 5′-Cp-N^2-dG-3′-R-(α)-CH$_3$-propyl-5′-Cp-N^2-dG-3′ Cross-linked Adduct 8a—Figure 3A shows the resonances arising from the Watson-Crick hydrogen bonded imino protons. The complete sequential NOE connectivity was observed between imino protons except at the terminal bases. The latter resonances were not observed due to rapid exchange with solvent. The imino resonance arising from the C^6•Y^{19} base pair was assigned at 12.6 ppm; the X^7•C^{18} base pair was assigned at 12.5 ppm. Each imino proton exhibited a strong NOE to an amino proton and that of opposite cytosine. Further, four strong A:T base parings were present, as evidenced by NOEs between thymine N3H protons and adenine H2 protons. These arose from base pairs T^3•A^{22}, A^4•T^{21}, A^8•T^{17}, and T^{10}•A^{15}. As shown in Figure 4A, X^7 N1H exhibited strong NOEs to C^{18} N^4H_a, the complementary nucleotide, and X^7 N^2H. It showed weak NOE crosspeaks to C^6 N^4H_a and Y^{19} N^2H. In contrast, Y^{19} N1H displayed strong NOEs to C^6 N^4H_a and Y^{19} N^2H, and weak crosspeaks to C^{18} N^4H_a and X^7 N^2H. A similar pattern of NOE intensities was observed between X^7 N1H and Y^{19} N1H to C^{18} N^4H_b and C^6 N^4H_b. In addition, X^7 N1H showed an NOE to A^8 H2 and T^{17} CH_3. The methyl protons of the cross-link had a stronger NOE to X^7 N1H than to Y^{19} N1H. The H_γ protons showed weak NOEs to X^7 N1H whereas H_α showed NOEs to both X^7 N1H and Y^{19} N1H.

(b) 5′-Cp-N^2-dG-3′-S-(α)-CH$_3$-propyl-5′-Cp-N^2-dG-3′ Cross-linked Adduct 8b—Figure 3B shows the resonances arising from the Watson-Crick hydrogen bonded imino protons. The complete sequential NOE connectivity was observed between imino protons of the duplex except at the terminal bases. The latter resonances were not observed due to rapid exchange with solvent. The imino resonance arising from the C^6•Y^{19} base pair was assigned at 12.5 ppm; the X^7•C^{18} base pair was assigned at 12.3 ppm. Each imino proton exhibited a strong NOE to the corresponding Watson-Crick hydrogen-bonded amino proton and to the hydrogen-bonded amino proton of the complementary cytosine, as shown in Figure 4B. Further, four strong A:T base parings were present, as evidenced by NOEs between thymine N3H protons and adenine H2 protons. These arose from base pairs T^3•A^{22}, A^4•T^{21}, A^8•T^{17},

and T^{10}•A^{15}. Additional NOEs were observable with a similar pattern as 5′-Cp-N^2-d<u>G</u>-3′- *R*-(α)-CH_3-propyl-5′-Cp-N^2-d<u>G</u>-3′ cross-linked Adduct. The H_α proton and methyl protons showed stronger crosspeaks to X^7 N1H than to Y^{19} N1H. On the other hand, the H_γ and H_β protons showed stronger crosspeaks to Y^{19} N1H than to X^7 N1H.

Assignments of the Cross-link Protons

(a) 5′-Cp-N^2-d<u>G</u>-3′-R-(α)-CH_3-propyl-5′-Cp-N^2-d<u>G</u>-3′ Cross-linked Adduct 8a—All cross-link protons were assigned (Figure 5A) from a combination of ^{1}H COSY and NOESY experiments. The CH_3 resonance was observed at 1.03 ppm. It exhibited a COSY crosspeak to a resonance at 3.82 ppm, assigned as the H_α resonance. The H_α proton manifested an additional crosspeak to a resonance at 1.82 ppm, assigned as arising from the $H_{\beta1}$ proton.[i] The $H_{\beta1}$ proton had a strong geminal coupling to a resonance at 1.63 ppm, arising from $H_{\beta2}$, and weak coupling to a resonance at 2.82 ppm, arising from $H_{\gamma2}$. The $H_{\gamma2}$ proton also had a strong geminal coupling to $H_{\gamma1}$ proton at 3.71 ppm. The $H_{\gamma2}$ and the H_α protons were the most deshielded, presumably due to the trans orientation with respect to the hydrogen-bonded N^2H of deoxyguanosines. All of the anticipated dipolar couplings were observed to other cross-link protons.

(b) 5′-Cp-N^2-d<u>G</u>-3′-S-(α)-CH_3-propyl-5′-Cp-N^2-d<u>G</u>-3′ Cross-linked Adduct 8b— All adduct protons were assigned (Figure 5B) from a combination of ^{1}H COSY, TOCSY, and NOESY experiments. The $H_{\beta1}\rightarrow H_{\beta2}$, $H_{\gamma1}\rightarrow H_{\gamma2}$ geminal couplings exhibited strong DQF-COSY crosspeaks, as did the $CH_3\rightarrow H_\alpha$ cross-peak. Different chemical shifts were observed as compared to the cross-link with *R* stereochemistry (Table 1). A major difference was the differential chemical shifts of the H_β protons. The $H_{\beta1}$ proton was observed at 1.09 ppm, while $H_{\beta2}$ was observed at 2.77 ppm. Also, H_α shifted upfield compared to its position in the cross-link with *R* stereochemistry.

Cross-link-DNA NOEs

(a) 5′-Cp-N^2-d<u>G</u>-3′-R-(α)-CH_3-propyl-5′-Cp-N^2-d<u>G</u>-3′ Cross-linked Adduct 8a— The CH_3 protons of the cross-link exhibited strong NOEs to A^8 H2, and A^8 H1′ (Figure 6A). The CH_3 protons showed weaker NOEs to X^7 H1′ and C^{20} H1′, and A^8 H2 and H4′. The $H_{\gamma1}$ and $H_{\gamma2}$ protons exhibited stronger NOEs to C^{20} H1′ as compared to the $H_{\beta1}$, $H_{\beta2}$, and H_α protons. Weak NOEs were observed between H_α and A^8 H1′ and X^7 H1′. Overall, this pattern of NOE intensities positioned the methyl group in the 3′ direction with respect to X^7.

(b) 5′-Cp-N^2-d<u>G</u>-3′-S-(α)-CH_3-propyl-5′-Cp-N^2-d<u>G</u>-3′ Cross-linked Adduct 8b— Figure 6B presents correlations among base protons in base pairs X^7•C^{18} and C^6•Y^{19}, including NOEs to adduct protons. The CH_3 protons showed an intense NOE to A^8 H1′, and strong NOEs to A^8 H2 and H4′. Weaker NOEs were observed from the CH_3 protons to X^7 H1′, X^7 H4′, A^8 H3′, and C^{20} H1′. Strong crosspeaks were observed between H_α and $H_{\gamma1}$ and C^{20} H1′. This pattern of NOEs suggested that the CH_3 group was oriented toward the 3′ direction with respect to nucleotide X^7, proximate to A^8 H1′ in the minor groove.

Chemical Shift Perturbations

(a) 5′-Cp-N^2-d<u>G</u>-3′-R-(α)-CH_3-propyl-5′-Cp-N^2-d<u>G</u>-3′ Cross-linked Adduct 8a— Figure S1 A,B in the Supporting Information compares the chemical shifts of the deoxyribose protons of the cross-linked duplex with those of the corresponding non-cross-linked duplex. The greatest changes were localized to the 5′-neighbor cytosine and X^7 H2′ proton. The other chemical shift perturbations of the base protons were consistently less than 0.1 ppm. The C^6 H1′ and C^{18} H1′ protons each shifted upfield by approximately 0.05 ppm, whereas the X^7 H1′

and Y^{19} H1′ protons were deshielded by approximately 0.02 ppm. These perturbations were similar to those observed for the propyl inter-strand cross-link (42).

(b) 5′-Cp-N^2-dG-3′-S-(α)-CH_3-propyl-5′-Cp-N^2-dG-3′ Cross-linked Adduct 8b— Figure S1 C,D in the Supporting Information compares the chemical shifts of the deoxyribose protons of the cross-linked duplex with those of the corresponding non-cross-linked duplex. The greatest changes were localized to the 5′-neighbor cytosine, and X^7 H2′. The largest difference was approximately 0.7 ppm for the 5′-neighbor C^6 H2′. The other chemical shift perturbations of the base protons were consistently less than 0.2 ppm. The C^6 H1′ and C^{18} H1′ protons each shifted upfield by approximately 0.05 ppm, whereas the X^7 H1′ and Y^{19} H1′ protons were deshielded by approximately 0.02 ppm. These chemical shift perturbations were similar to those observed for the propyl inter-strand cross-link (42)

Torsion Angles

(a) 5′-Cp-N^2-dG-3′-R-(α)-CH_3-propyl-5′-Cp-N^2-dG-3′ Cross-linked Adduct 8a— The NOE data suggested that all of the glycosyl torsion angles were in the anti conformation. Deoxyribose pseudorotations were estimated from $^3J_{HH}$ coupling constants (45). The $^3J_{H1'-H2'}$ and $^3J_{H1'-H2''}$ coupling constants were measured from E-COSY experiments (46), while the $^3J_{H2''-H3'}$ and $^3J_{H3'-H4'}$ coupling constants were determined from DQF-COSY experiments. The data were fit to curves relating the coupling constants to the pseudorotation (*P*), sugar pucker amplitude (ϕ), and the percentage S-type conformation. The pseudorotation and amplitude ranges were converted to the five dihedral angles ν_0 to $\nu_4$47). The data were consistent with all deoxyribose pseudorotations being in the C2′-endo range. The ^{31}P spectrum showed no unusual chemical shifts, suggesting that the backbone was not perturbed.

(b) 5′-Cp-N^2-dG-3′-S-(α)-CH_3-propyl-5′-Cp-N^2-dG-3′ Cross-linked Adduct 8b— The NOE data suggested that all of the glycosyl torsion angles were in the *anti* conformation, and the deoxyribose sugars were in the C2′-endo conformation (47). The ^{31}P spectrum showed no unusual chemical shifts, suggesting that the backbone was not perturbed.

Structural Refinement

(a) 5′-Cp-N^2-dG-3′-R-(α)-CH_3-propyl-5′-Cp-N^2-dG-3′ Cross-linked Adduct 8a—A-form and B-form DNA starting structures were constructed, with the cross-link between X^7 and Y^{19}. The cross-link was parameterized for the AMBER 8.0 program as shown in Figure S2 of the Supporting Information. There was a total of 303 distance restraints generated from the NOE data using the program MARDIGRAS (34, 48). In addition, 52 empirical Watson-Crick restraints were incorporated in rMD calculations.

The precision of the rMD calculations was monitored by pairwise rmsd analysis of the emergent structures. Figure S3 A in the Supporting Information shows a stereoview of structures emerging from the rMD calculations. The rmsd between the A-DNA and B-DNA starting structures was 6.4 Å. The pairwise rmsd between averaged structures from IniA and IniB was 1.4 Å. The final refined structure was compared to the starting A-DNA and B-DNA structures. It exhibited a rmsd of 2.6 Å to the B-DNA starting structure, and a rmsd of 4.3 Å to the A-DNA starting structure. This indicated that the convergent structures more closely resembled B-DNA than A-DNA. Detailed results are listed in Table 2.

The accuracies of the structures that emerged from the rMD calculations were evaluated by complete relaxation matrix analysis, using the program CORMA. Figure S4 A,B in the Supporting Information presents sixth root $R_1^{\ x}$ residuals at each nucleotide, in comparison with experimental NOE data obtained at a mixing time of 150 ms. The overall $R_1^{\ x}$ residual for the cross-linked oligodeoxynucleotide was 7.04 5 10^{-2}. The overall intra-nucleotide $R_1^{\ x}$

residual was 6.47 5 10^{-2}, and the overall inter-nucleotide $R_1{}^x$ residual was 7.72 5 10^{-2}. These values indicated agreement between the refined structures and the NOESY data.

(b) 5′-Cp-N^2-dG-3′-S-(α)-CH$_3$-propyl-5′-Cp-N^2-dG-3′ Cross-linked Adduct 8b—A-form and B-form DNA starting structures were constructed, as described above for cross-linked adduct **8a**. A total of 364 distance restraints were generated from the NOE data using the program MARDIGRAS (34,48). A total of 52 empirical Watson-Crick restraints were incorporated in rMD calculations.

Figure S3 B in the Supporting Information shows a stereoview of convergent structures emerging from the rMD calculations. The rmsd between A-DNA and B-DNA starting structures was 6.4 Å. The pairwise rmsd between averaged structures as compared to the initial A- and B-DNA starting structures was 1.6 Å. The final averaged and energy-minimized structure was compared to starting structure and a 2.5 Å rmsd was observed between the initial B-form starting structure and rMD_{avg}, while a 4.3 Å rmsd was observed between the initial A-form starting structure and rMD_{avg}. Detailed results are listed in Table 2.

The accuracies of the structures that emerged from the rMD calculations were evaluated by complete relaxation matrix analysis, using the program CORMA. Figure S4 C,D in the Supporting Information presents sixth root $R_1{}^x$ residuals at each nucleotide, in comparison with experimental NOE data obtained at a mixing time of 60 ms. The overall $R_1{}^x$ residual for the cross-linked oligodeoxynucleotide was 5.70 5 10^{-2}. The overall intra-nucleotide $R_1{}^x$ residual was 5.03 5 10^{-2}, and the overall inter-nucleotide $R_1{}^x$ residual was 7.03 5 10^{-2}. These values indicated agreement between the refined structures and the NOESY data.

Structure of the 5′-Cp-N^2-dG-3′-R-(α)-CH$_3$-propyl-5′-Cp-N^2-dG-3′ Cross-linked Adduct 8a

Figure 7 A shows the refined structure of the inter-strand cross-link from the minor groove. The *R*-(α)-CH_3 group oriented in the 3′ direction with respect to X^7. It faced toward T^{17} in the complementary strand and was centered within the minor groove. This allowed the *R*-(α)-CH_3 group to be easily accommodated within the minor groove. It also allowed the cross-linked oligodeoxynucleotide to maintain Watson-Crick hydrogen bonds and normal base stacking interactions at the tandem cross-linked base pairs C^6•Y^{19} and X^7•C^{18} (Figure 8 A). The conformation of the propyl group is shown in a Newman projection in Figure 9 A. At the C_α-C_β bond, H_α was *trans* to $H_{\beta1}$ and *gauche* with respect to $H_{\beta2}$, consistent with the large $H_\alpha \rightarrow H_{\beta1}$ ^3J coupling constant and smaller $H_\alpha \rightarrow H_{\beta2}$ ^3J coupling constant. At the C_β-C_γ bond, $H_{\gamma2}$ was trans to $H_{\beta1}$ and gauche with respect to $H_{\beta2}$, consistent with the large $H_{\gamma2} \rightarrow H_{\beta1}$ ^3J coupling constant and smaller $H_{\gamma2} \rightarrow H_{\beta2}$ ^3J coupling constant.

Structure of the 5′-Cp-N^2-dG-3′-R-(α-CH$_3$-propyl-5′-Cp-N^2-dG-3′ Cross-linked Adduct 8b

Figure 7 B shows the refined structure of the inter-strand cross-link from the minor groove. The *S*-(α)-CH_3 group oriented in the 3′ direction with respect to X^7. It faced toward A^8 and was within the minor groove. This created a clash between the CH_3 and the right handed helical trajectory of the minor groove, as predicted by modeling studies (49). Nevertheless, the cross-linked oligodeoxynucleotide maintained Watson-Crick hydrogen bonds and reasonable base stacking at the tandem cross-linked base pairs C^6•Y^{19} and X^7•C^{18}, shown in Figure 8 B. The conformation of the propyl group is shown in a Newman projection in Figure 9 B. At the C_α-C_β bond, $H_{\gamma1}$ was *trans* to $H_{\beta2}$ and *gauche* with respect to $H_{\beta1}$, consistent with the large $H_{\gamma1} \rightarrow H_{\beta2}$ ^3J coupling constant and smaller observed $H_{\gamma1} \rightarrow H_{\beta1}$ ^3J coupling constant. At the C_β-C_γ bond, H_α was trans to $H_{\beta2}$ and gauche with respect to $H_{\beta1}$, consistent with the large $H_\alpha \rightarrow H_{\beta2}$ ^3J coupling constant and smaller $H_\alpha \rightarrow H_{\beta1}$ ^3J coupling constant. Consequently, the protons of the propyl cross-link were oriented differently than in the corresponding cross-link

with *R* stereochemistry of the CH_3 group, consistent with their differential chemical shifts in the two stereoisomeric cross-links (Figure 5).

DISCUSSION

The 5′-Cp-N^2-dG-3′- *R*-(α)-CH_3-propyl-5′- Cp-N^2-dG-3′ and 5′- Cp-N^2-dG-3′-*S*-(α)-CH_3-propyl-5′-Cp-N^2-dG-3′ cross-links **8a** and **8b** provided chemically stable surrogates for carbinolamine cross-links **5a** and **5b** arising from the crotonaldehyde and acetaldehyde-derived *R*- and *S*-α-CH_3-γ-OH-1,N^2-propanodeoxyguanosine adducts **2a** and **2b** in duplex DNA (49). Structural studies on the reduced cross-links **8a** and **8b** provided an opportunity to probe for an explanation to the observation that inter-strand cross-link formation in the 5′-CpG-3′ sequence is dependent upon adduct stereochemistry, favoring the *R*-α-CH_3-γ-OH-1,N^2-propanodeoxyguanosine adduct **2a**.

Structures of the 5′-Cp-N^2-dG-3′-R-(α)-CH_3-propyl-5′-Cp-N^2-dG-3′ and 5′-Cp-N^2-dG-3′- S-(α)-CH_3-propyl-5′-Cp-N^2-dG-3′ Cross-links 8a and 8b

The results reveal that the 5′-Cp-N^2-dG-3′- *R*-(α)-CH_3-propyl-5′-Cp-N^2-dG-3′ cross-link **8a** is thermodynamically more stable than is the 5′-Cp-N^2-dG-3′-*S*-(α)-CH_3-propyl-5′-Cp-N^2-dG-3′ cross-link **8b**. While both cross-links were accommodated within the minor groove of the duplex, with small distortions of DNA structure, the T_m of the 5′-Cp-N^2-dG-3′- *S*-(α)-CH_3-propyl-5′-Cp-N^2-dG-3′ cross-link **8b** was lower (Figure 1). The differential melting of the two cross-links correlates specifically with the tandem cross-linked base pairs C^6•Y^{19} and X^7•C^{18}. The Watson-Crick hydrogen bonding of these two base pairs is more thermally stable in the 5′-Cp-N^2-dG-3′-*R*-(α)-CH_3-propyl-5′-Cp-N^2-dG-3′ cross-link **8a** than the 5′-Cp-N^2-dG-3′-*S*-(α)-CH_3-propyl-5′-Cp-N^2-dG-3′ cross-link **8b**.

The structural studies suggest that the differential thermal stabilities of the two cross-links are due to stereospecific differences in the conformation of the (α)-CH_3 group. For the 5′-Cp-N^2-dG-3′-*R*-(α)-CH_3-propyl-5′-Cp-N^2-dG-3′ cross-link **8a**, the (α)-CH_3 group oriented in the 3′ direction within the minor groove, and did not interfere with the right handed geometry of the minor groove. In contrast, the 3′-orientation of the α-CH_3 group for cross-link **8b** did interfere at X^7 and A^8 with the right handed geometry of the minor groove. This necessitated the conformational reorganization of cross-link **8b** as compared to cross-link **8a**, so as to place the (α)-CH_3 group as far as possible from the floor of the minor groove at X^7. The differential patterns of ^3J coupling constants in the ^{1}H NMR spectra corroborated the differential conformations of the three-carbon cross-links. For the 5′-Cp-N^2-dG-3′-*R*-(α)-CH_3-propyl-5′-Cp-N^2-dG-3′ cross-link **8a**, the $H_{\beta 1}\rightarrow H_{\gamma 2}$ and $H\alpha\rightarrow H_{\beta 1}$ crosspeaks exhibited large ^3J coupling constants consistent with their *trans* orientation. In addition, for cross-link **8b**, the $H_{\beta 2}\rightarrow H_{\gamma 1}$ and $H_\alpha\rightarrow H_{\beta 2}$ crosspeaks exhibited large ^3J coupling constants consistent with their *trans* orientation. Likewise, the different chemical shifts of the propyl protons in the stereoisomeric cross-links were consistent with the conclusion that the corresponding protons in the two cross-links were in different environments.

Molecular modeling had predicted that carbinolamine cross-links **5a** and **5b**, with sp^3 hybridization at the γ-carbon, allowed the tandem cross-linked C^6•Y^{19} and X^7•C^{18} base pairs to maintain Watson-Crick hydrogen bonding (49). In contrast, dehydration of the carbinolamine to the imine (Schiff base) cross-link would result in sp^2 hybridization and loss of Watson-Crick hydrogen bonding. The 5′-Cp-N^2-dG-3′-*R*-(α)-CH_3-propyl-5′-Cp-N^2-dG-3′ and 5′-Cp-N^2-dG-3′-*S*-(α)-CH_3-propyl-5′-Cp-N^2-dG-3′ cross-links **8a** and **8b** lack the γ-OH group present in the native cross-links. However, it may be inferred from the present results that the sp^3 hybridization at the γ-carbon of the cross-link does allow the exocyclic amine proton at Y^{19} to participate in Watson-Crick hydrogen bonding, with minimal perturbation of the DNA duplex, irrespective of *R*- vs. *S*-stereochemistry at the (α)-CH_3 group (Figure 8). In

both reduced crosslinks **8a** and **8b**, the exocyclic amine protons at both X^7 and Y^{19} were observed in the NMR spectra, and for both reduced crosslinks **8a** and **8b**, the exocyclic amine protons at both X^7 and Y^{19} exhibited NOEs to the corresponding X^7 N1H and Y^{19} N1H imino protons, consistent with the conclusion that they were participating in hydrogen bonds. This is indicative of Watson-Crick hydrogen bonds at both C^6•Y^{19} and X^7•C^{18}, for both reduced crosslinks **8a** and **8b**. This is consistent with studies of other N^2-dG adducts such as those arising from mitomycin C, anthramycin, and benzo[*a*]pyrene diol epoxides that leave the deoxyguanosine exocyclic amine proton available to participate in Watson-Crick hydrogen bonding (50–52).

Comparison with the 5′-Cp-N^2-dG-3′-Propyl -5′-Cp-N^2-dG-3′ Cross-link

A similar strategy was used by Dooley et al. (42,53) to examine the reduced 5′-Cp-N^2-dG-3′-propyl-5′-Cp-N^2-dG-3′ and 5′-N^2-dGpC-3′-propyl-5′-N^2-dGpC-3′ cross-links in the 5′-CpG-3′ vs. 5′-GpC-3′ sequences. In the 5′-CpG-3′ sequence, the Dooley et al. structure (42) differed from those of the 5′-Cp-N^2-dG-3′-*R*-(α)-CH_3-propyl-5′-Cp-N^2-dG-3′ and 5′-Cp-N^2-dG-3′-*S*-(α)-CH_3-propyl-5′-Cp-N^2-dG-3′ cross-links **8a** and **8b** reported herein. In the 5′-Cp-N^2-dG-3′-propyl-5′-Cp-N^2-dG-3′ cross-link, their three carbon cross-link was accommodated by unwinding the duplex at the cross-linked base pairs to produce a bulge. The tethered guanines were approximately in the same plane. Consequently, Watson-Crick hydrogen bonding was disrupted at the tandem cross-linked base pairs. The formation of a bulge accommodated the extended chain conformation of the linker between the two deoxyguanosines in the 5′-CpG-3′ sequence. In the extended chain conformation, the exocyclic nitrogens of each deoxyguanosine were in an *anti* orientation with respect to their respective γ-carbon atoms of the propyl cross-link (42). For the 5′-Cp-N^2-dG-3′-*R*-(α)-CH_3-propyl-5′-Cp-N^2-dG-3′ and 5′-Cp-N^2-dG-3′- *S*-(α)-CH_3-propyl-5′-Cp-N^2-dG-3′ cross-links **8a** and **8b**, the exocyclic nitrogens of each deoxyguanosine were instead in the *gauche* orientation with respect to their respective γ-carbon atoms of the propyl cross-link (Figure 9). Molecular modeling suggested that the presence of either stereoisomer of the (α)-CH_3 group created steric strain in the extended chain conformation, which may explain the observed *gauche* orientation of the exocyclic nitrogens of each deoxyguanosine with respect to their respective Ω-carbon atoms in the crotonaldehyde-derived cross-links.

Kinetics of Inter-strand Cross-link Formation by the R- or S-α-CH_3-γ-OH-PdG Adducts 2a and 2b

In addition to being energetically disfavored with respect to the inter-strand cross-link formed by the *R*-α-CH_3-γ-OH-PdG adduct **2a**, the rate of cross-link formation by the *S*-α-CH_3-γ-OH-PdG adduct **2b** is slower. Twenty days after annealing 5′-d(GCTAGCXAGTCC)-3′•5′-d(GGACTCYCTAGC)-3′ (X = *R*- or *S*-*a*-CH_3-γ-^{13}C-OH-PdG; Y = $^{15}N^2$-dG) at pH 7 and 37 °C, spectroscopically detectable amounts of an inter-strand carbinolamine cross-link were observed only for the *R*-α-CH_3-γ-OH-PdG adduct **2a** (25). However, treatment of the oligodeoxynucleotide containing the *S*-*a*-CH_3-γ-OH-PdG adduct **2b** with $NaCNBH_3$ successfully trapped the reduced inter-strand cross-link **8b** (23), suggesting that imine cross-link **4b** was in fact present, below the level of NMR detection. Subsequent ^{13}C HSQC NMR studies, in which the sample was monitored at 37 °C for seventy days, revealed the presence of the inter-strand 5′-CpG-3′ carbinolamine cross-link **5b** derived from the *S*-α-CH_3-γ-^{13}C-OH-PdG adduct **2b**. Thus, at pH 7 and 37 °C, twenty days were insufficient to allow the duplex containing the *S*-α-CH_3-γ-^{13}C-OH-PdG adduct **2b** to reach equilibrium.

Previous studies revealed a structural basis for the slow rate of inter-strand cross-link formation by the *S*-α-CH_3-γ-OH-PdG adduct **2b** (54). Within the minor groove, the aldehyde moiety of adduct **3b** oriented in the 3′ direction, while the 1(*S*) methyl group oriented in the 5′ direction. This positioned the aldehyde distal to the G^{19} amino group hindering formation of the 5′-

CpG-3′ inter-strand cross-link (54). Thus, we conclude that the formation of inter -strand cross-links by the N^2-(*S*-α-CH_3-γ-OH-1,N^2-propano-2′)-dG adduct **2b** is not only energetically disfavored, but also kinetically disfavored. Both the energetics and the kinetics of cross-link formation are modulated by stereochemistry at the (α)-CH_3 group.

Biological Implications

The crotonaldehyde and acetaldehyde-derived *R*- and *S*-α-CH_3-γ-OH-1,N^2-propanodeoxyguanosine adducts **2a** and **2b** have both been isolated from mammalian tissues, including human cells (11–13). Both are anticipated to contribute to the etiology of human mutagenesis and cancer. When DNA containing adducts **2a** and **2b** was introduced into human xeroderma pigmentosum A (XPA) cells and examined as to replication (55), the major miscoding events in the XPA cells for both adducts were G→T transversions, with G→A transitions also being observed for adduct **2a**, whereas G→C transversions were the second most common events for adduct **2b**. The site-specific mutagenesis of adducts **2a** and **2b** has also been examined in COS-7 cells, also showing primarily G→T transversions (56). It is generally thought that the propensity of cyclic adducts **2a** or **2b** to undergo ring opening to the N^2-(3-oxopropyl)-dG aldehydes **3a** or **3b** (Chart 1) facilitates lesion bypass, as reported for the acrolein-derived γ-OH-PdG adduct (57–61). On the other hand, in duplex DNA, incomplete conversion of crotonaldehyde-derived adducts **2a** and **2b** to aldehydes **3a** and **3b** or hydrated aldehydes **4a** and **4b** may block DNA replication, possibly reducing their mutagenicity. The formation of inter-strand carbinolamine cross-link **5a** by *R*-α-CH_3-γ-OH-1,N^2-propanodeoxyguanosine adduct **2a** might also block DNA replication, and thus reduce its mutagenicity as compared to *S*-α-CH_3-γ-OH-1,N^2-propanodeoxyguanosine adduct **2b**. The equilibrium chemistry of adducts **2a** and **2b**, and in particular, the chemical stability of carbinolamine cross-link **5a** (Chart 1), within DNA replication or repair complexes is of considerable interest; Liu et al. (26) report that cross-links **5a** and **5b** were stable during construction of site-specifically modified plasmids, but concluded that in *E. coli*, proficient nucleotide excision repair was absolutely required to repair cross-link **8a**. Thus, *E. coli* transformants obtained using cross-links **5a** and **5b** were interpreted as arising from some proportion of native cross-links that had reverted to the respective monoadducts. However, in nucleotide excision repair-deficient human XPA cells, residual repair of cross-link **8a** was observed (26), which suggested the presence of a replication-coupled NER-independent cross-link repair pathway (62), e.g., the proposed ERCC1-XPF endonuclease replication fork cross-link repair pathway (63,64). In XPA cells, the primary mutations induced as a consequence of error-prone repair of reduced cross-link **8a** were low levels of G→T transversions targeting the cross-linked dG in the lagging strand template (26). The specific polymerases responsible for trans-lesion synthesis remain to be identified, but Y-family polymerase η (65) and as well, pol ζ (66,67), are candidates. Washington et al. (68,69) showed that the Y-polymerase pol ι in conjunction with pol κ, or Rev 1 in combination with pol ζ could efficiently bypass the acrolein-derived γ-OH-PdG adduct. Minko et al. (70) showed that pol η could bypass the γ-OH-PdG adduct to a lesser extent. It seems plausible that these error-prone polymerases might also bypass equilibrium mixtures ofcrotonaldehyde and acetaldehyde derived monoadducts **2a**, **3a**, **4a**, or **2b**, **3b**, **4b**, or partially excised intermediates arising from replication-coupled repair of inter-strand cross-links **5a** or **5b**.

Supplementary Material

Refer to Web version on PubMed Central for supplementary material.

ACKNOWLEDGEMENTS

We thank Dr. Jarrod Smith for suggestions regarding AMBER calculations. This work was supported by NIH grant ES-05335 (T.M.H., R.S.L., C.J.R., and M.P.S.). Funding for the NMR spectrometers was supplied by Vanderbilt

University; by NIH grant RR-05805, and the Vanderbilt Center in Molecular Toxicology, ES-00267. The Vanderbilt-Ingram Cancer Center is supported by NIH grant CA-68485. Portions of this work were presented at the 230th National meeting of the American Chemical Society, August 28-September 1, 2005, Washington, DC.

REFERENCES

1. Czerny C, Eder E, Runger TM. Genotoxicity and mutagenicity of the α,β-unsaturated carbonyl compound crotonaldehyde (butenal) on a plasmid shuttle vector. Mutat. Res 1998;407:125–134. [PubMed: 9637241]
2. Chung FL, Tanaka T, Hecht SS. Induction of liver tumors in F344 rats by crotonaldehyde. Cancer Res 1986;46:1285–1289. [PubMed: 3002613]
3. Chung FL, Hecht SS. Formation of cyclic 1,N^2--adducts by reaction of deoxyguanosine with α-acetoxy-N- nitrosopyrrolidine, 4-(carbethoxynitrosamino)butanal, or crotonaldehyde. Cancer Res 1983;43:1230–1235. [PubMed: 6825094]
4. Eder E, Schuler D, Budiawan. Cancer risk assessment for crotonaldehyde and 2-hexenal: An approach. IARC Sci. Publ 1999;150:219–232. [PubMed: 10626223]
5. Chung FL, Zhang L, Ocando JE, Nath RG. Role of 1,N^2-propanodeoxyguanosine adducts as endogenous DNA lesions in rodents and humans. IARC Sci. Publ 1999;150:45–54. [PubMed: 10626207]
6. Wang M, McIntee EJ, Cheng G, Shi Y, Villalta PW, Hecht SS. Identification of DNA adducts of acetaldehyde. Chem. Res. Toxicol 2000;13:1149–1157. [PubMed: 11087437]
7. Wang M, McIntee EJ, Cheng G, Shi Y, Villalta PW, Hecht SS. Identification of paraldol-deoxyguanosine adducts in DNA reacted with crotonaldehyde. Chem. Res. Toxicol 2000;13:1065–1074. [PubMed: 11080056]
8. Wang M, McIntee EJ, Cheng G, Shi Y, Villalta PW, Hecht SS. A Schiff base is a major DNA adduct of crotonaldehyde. Chem. Res. Toxicol 2001;14:423–430. [PubMed: 11304131]
9. International Agency for Research on Cancer. Re-evaluation of some organic chemicals, hydrazine and hydrogen peroxide, IRC Monographs on the Evaluation of Carcinogenic Risks to Humans; IARC Sci. Publ. 1999. p. 109-125.
10. Lao Y, Hecht SS. Synthesis and properties of an acetaldehyde-derived oligonucleotide interstrand cross-link. Chem. Res. Toxicol 2005;18:711–721. [PubMed: 15833031]
11. Chung FL, Nath RG, Nagao M, Nishikawa A, Zhou GD, Randerath K. Endogenous formation and significance of 1,N^2-propanodeoxyguanosine adducts. Mutat. Res 1999;424:71–81. [PubMed: 10064851]
12. Budiawan, Eder E. Detection of 1,N^2-propanodeoxyguanosine adducts in DNA of Fischer 344 rats by an adapted ^{32}P-post-labeling technique after per os application of crotonaldehyde. Carcinogenesis 2000;21:1191–1196. [PubMed: 10837009]
13. Zhang S, Villalta PW, Wang M, Hecht SS. Analysis of crotonaldehyde- and acetaldehyde-derived 1,N^2-propanodeoxyguanosine adducts in DNA from human tissues using liquid chromatography electrospray ionization tandem mass spectrometry. Chem. Res. Toxicol 2006;19:1386–1392. [PubMed: 17040109]
14. Nath RG, Chung FL. Detection of exocyclic 1,N^2- propanodeoxyguanosine adducts as common DNA lesions in rodents and humans. Proc. Natl. Acad. Sci. USA 1994;91:7491–7495. [PubMed: 8052609]
15. Nath RG, Ocando JE, Chung FL. Detection of 1, N^2- propanodeoxyguanosine adducts as potential endogenous DNA lesions in rodent and human tissues. Cancer Res 1996;56:452–456. [PubMed: 8564951]
16. Treitman RD, Burgess WA, Gold A. Air contaminants encountered by firefighters. Am. Ind. Hyg. Assoc. J 1980;41:796–802. [PubMed: 7457369]
17. Izard C, Valadaud-Barrieu D, Fayeulle JP, Testa A. Effect of smoking-machine parameters on the genotoxic activity of cigarette gas phase, estimated on human lymphocyte and yeast (author's transl). Mutat. Res 1980;77:341–344. [PubMed: 6990251]
18. Chung FL, Chen HJ, Nath RG. Lipid peroxidation as a potential endogenous source for the formation of exocyclic DNA adducts. Carcinogenesis 1996;17:2105–2111. [PubMed: 8895475]

19. Hecht SS, Upadhyaya P, Wang M. Reactions of α-acetoxy-N-nitrosopyrrolidine and crotonaldehyde with DNA. IARC Sci. Publ 1999;150:147–154. [PubMed: 10626216]
20. Kozekov ID, Nechev LV, Sanchez A, Harris CM, Lloyd RS, Harris TM. Interchain cross-linking of DNA mediated by the principal adduct of acrolein. Chem. Res. Toxicol 2001;14:1482–1485. [PubMed: 11712904]
21. Nechev LV, Kozekov I, Harris CM, Harris TM. Stereospecific synthesis of oligonucleotides containing crotonaldehyde adducts of deoxyguanosine. Chem. Res. Toxicol 2001;14:1506–1512. [PubMed: 11712908]
22. Nechev LV, Zhang M, Tsarouhtsis D, Tamura PJ, Wilkinson AS, Harris CM, Harris TM. Synthesis and characterization of nucleosides and oligonucleotides bearing adducts of butadiene epoxides on adenine N^6 and guanine N^2. Chem. Res. Toxicol 2001;14:379–388. [PubMed: 11304126]
23. Kozekov ID, Nechev LV, Moseley MS, Harris CM, Rizzo CJ, Stone MP, Harris TM. DNA interchain cross-links formed by acrolein and crotonaldehyde. J. Am. Chem. Soc 2003;125:50–61. [PubMed: 12515506]
24. Kurtz AJ, Lloyd RS. 1,N^2-Deoxyguanosine adducts of acrolein, crotonaldehyde, and trans-4-hydroxynonenal cross-link to peptides via Schiff base linkage. J. Biol. Chem 2003;278:5970–5976. [PubMed: 12502710]
25. Cho YJ, Wang H, Kozekov ID, Kurtz AJ, Jacob J, Voehler M, Smith J, Harris TM, Lloyd RS, Rizzo CJ, Stone MP. Stereospecific formation of interstrand carbinolamine DNA cross-links by crotonaldehyde- and acetaldehyde-derived α-CH_3-γ-OH-1, N^2 -propano-2′- deoxyguanosine adducts in the 5′-CpG-3′ sequence. Chem. Res. Toxicol 2006;19:195–208. [PubMed: 16485895]
26. Liu X, Lao Y, Yang IY, Hecht SS, Moriya M. Replication-coupled repair of crotonaldehyde/acetaldehyde-induced guanine-guanine interstrand cross-links and their mutagenicity. Biochemistry 2006;45:12898–12905. [PubMed: 17042508]
27. Borer, PN. Handbook of Biochemistry and Molecular Biology. 1 ed.. Cleveland: CRC Press; 1975.
28. Campbell TG, Urbach FL. Synthesis and characterization of nickel (II) complexes of neutral, tetradentate Schiff-base ligands derived from 1,3-diamines. Inorg. Chem 1973;12:1836–1840.
29. Piotto M, Saudek V, Sklenar V. Gradient-tailored excitation for single-quantum NMR spectroscopy of aqueous solutions. J. Biomol. NMR 1992;2:661–665. [PubMed: 1490109]
30. Piantini U, Sorensen OW, Ernst RR. Multiple quantum filters for elucidating NMR coupling networks. J. Am. Chem. Soc 1982;104:6800–6801.
31. Rance M, Sorensen OW, Bodenhausen G, Wagner G, Ernst RR, Wuthrich K. Improved spectral resolution in COSY ^{1}H NMR spectra of proteins via double quantum filtering. Biochem. Biophys. Res. Comm 1983;177:479–485. [PubMed: 6661238]
32. Delaglio F, Grzesiek S, Vuister GW, Zhu G, Pfeifer J, Bax A. NMRPipe: A multidimensional spectral processing system based on UNIX pipes. J. Biomol. NMR 1995;6:277–293. [PubMed: 8520220]
33. Keepers JW, James TL. A theoretical study of distance determination from NMR. Two-dimensional nuclear Overhauser effect spectra. J. Magn. Reson 1984;57:404–426.
34. Borgias BA, James TL. MARDIGRAS--a procedure for matrix analysis of relaxation for discerning geometry of an aqueous structure. J. Magn. Reson 1990;87:475–487.
35. Liu H, Tonelli M, James TL. Correcting NOESY cross-peak intensities for partial relaxation effects enabling accurate distance information. J. Magn. Reson. B 1996;111:85–89. [PubMed: 8620288]
36. Case, DA.; Pearlman, DA.; Caldwell, JW.; Cheatham, TE., III; Wang, J.; Ross, WS.; Simmerling, CL.; Darden, TA.; Merz, KM.; Stanton, RV.; Cheng, AL.; Vincent, JJ.; Crowley, M.; Tsui, V.; Gohlke, H.; Radmer, RJ.; Duan, Y.; Pitera, J.; Massova, I.; Seibel, GL.; Singh, UC.; Weiner, PK.; Kollman, PA. AMBER 8.0. San Francisco, CA: University of California; 2002.
37. Arnott S, Hukins DWL. Optimised parameters for A-DNA and B-DNA. Biochem. Biophys. Res. Comm 1972;47:1504–1509. [PubMed: 5040245]
38. Frisch, MJ.; Trucks, GW., et al. GAUSSIAN. Pittsburgh, PA: Gaussian, Inc.;
39. Bashford D, Case DA. Generalized Born models of macromolecular solvation effects. Annu. Rev. Phys. Chem 2000;51:129–152. [PubMed: 11031278]
40. Tsui V, Case DA. Theory and applications of the generalized Born solvation model in macromolecular simulations. Biopolymers 2000;56:275–291. [PubMed: 11754341]

41. Lu XJ, Olson WK. 3DNA: A software package for the analysis, rebuilding and visualization of three-dimensional nucleic acid structures. Nucleic Acids Res 2003;31:5108–5121. [PubMed: 12930962]
42. Dooley PA, Tsarouhtsis D, Korbel GA, Nechev LV, Shearer J, Zegar IS, Harris CM, Stone MP, Harris TM. Structural studies of an oligodeoxynucleotide containing a trimethylene interstrand cross-link in a 5′-(CpG) motif: Model of a malondialdehyde cross-link. J. Am. Chem. Soc 2001;123:1730–1739. [PubMed: 11456774]
43. Patel DJ, Shapiro L, Hare D. DNA and RNA: NMR studies of conformations and dynamics in solution. Q. Rev. Biophys 1987;20:35–112. [PubMed: 2448843]
44. Reid BR. Sequence-specific assignments and their use in NMR studies of DNA structure. Q. Rev. Biophys 1987;20:2–28.
45. Salazar M, Fedoroff OY, Miller JM, Ribeiro NS, Reid BR. The DNA strand in DNA:RNA hybrid duplexes is neither B-form nor A-form in solution. Biochemistry 1993;32:4207–4215. [PubMed: 7682844]
46. Griesinger G, Sorensen OW, Ernst RR. Two-dimensional correlation of connected NMR transitions. J. Am. Chem. Soc 1985;107:6394–6396.
47. Kim SG, Lin LJ, Reid BR. Determination of nucleic acid backbone conformation by ^{1}H NMR. Biochemistry 1992;31:3564–3574. [PubMed: 1373647]
48. Liu H, Spielmann HP, Ulyanov NB, Wemmer DE, James TL. Interproton distance bounds from 2D NOE intensities: Effect of experimental noise and peak integration errors. J. Biomol. NMR 1995;6:390–402. [PubMed: 8563467]
49. Cho YJ, Kim HY, Huang H, Slutsky A, Minko IG, Wang H, Nechev LV, Kozekov ID, Kozekova A, Tamura P, Jacob J, Voehler M, Harris TM, Lloyd RS, Rizzo CJ, Stone MP. Spectroscopic characterization of interstrand carbinolamine cross-links formed in the 5′-CpG-3′ sequence by the acrolein-derived γ- OH-1,N^2-propano-2′- deoxyguanosine DNA adduct. J. Am. Chem. Soc 2005;127:17686–17696. [PubMed: 16351098]
50. Kozack RE, Loechler EL. Molecular modeling of the conformational complexity of (+)-*anti*-B[*a*]PDE- adducted DNA using simulated annealing. Carcinogenesis 1997;18:1585–1593. [PubMed: 9276634]
51. Kopka ML, Goodsell DS, Baikalov I, Grzeskowiak K, Cascio D, Dickerson RE. Crystal structure of a covalent DNA-drug adduct: Anthramycin bound to C-C-A-A-C-G-T-T-G-G and a molecular explanation of specificity. Biochemistry 1994;33:13593–13610. [PubMed: 7947769]
52. Norman D, Live D, Sastry M, Lipman R, Hingerty BE, Tomasz M, Broyde S, Patel DJ. NMR and computational characterization of mitomycin cross-linked to adjacent deoxyguanosines in the minor groove of the d(T-A-C-G-T-A):d(T-A-C-G-T-A) duplex. Biochemistry 1990;29:2861–2875. [PubMed: 2346750]
53. Dooley PA, Zhang M, Korbel GA, Nechev LV, Harris CM, Stone MP, Harris TM. NMR determination of the conformation of a trimethylene interstrand cross-link in an oligodeoxynucleotide duplex containing a 5′-d(GpC) motif. J. Am. Chem. Soc 2003;125:62–72. [PubMed: 12515507]
54. Cho YJ, Wang H, Kozekov ID, Kozekova A, Kurtz AJ, Jacob J, Voehler M, Smith J, Harris TM, Rizzo CJ, Lloyd RS, Stone MP. Orientation of the crotonaldehyde-derived N^2-[3-oxo- 1(*S*)-methyl-propyl]-dG DNA adduct hinders interstrand cross-link formation in the 5′-CpG-3′ sequence. Chem. Res. Toxicol 2006;19:1019–1029. [PubMed: 16918240]
55. Stein S, Lao Y, Yang IY, Hecht SS, Moriya M. Genotoxicity of acetaldehyde- and crotonaldehyde-induced 1,N^2-propanodeoxyguanosine DNA adducts in human cells. Mutat. Res 2006;608:1–7. [PubMed: 16797223]
56. Fernandes PH, Kanuri M, Nechev LV, Harris TM, Lloyd RS. Mammalian cell mutagenesis of the DNA adducts of vinyl chloride and crotonaldehyde. Environ. Mol. Mutagen 2005;45:455–459. [PubMed: 15690339]
57. Yang IY, Hossain M, Miller H, Khullar S, Johnson F, Grollman A, Moriya M. Responses to the major acrolein-derived deoxyguanosine adduct in *Escherichia coli*. J. Biol. Chem 2001;276:9071–9076. [PubMed: 11124950]
58. Yang IY, Chan G, Miller H, Huang Y, Torres MC, Johnson F, Moriya M. Mutagenesis by acrolein-derived propanodeoxyguanosine adducts in human cells. Biochemistry 2002;41:13826–13832. [PubMed: 12427046]

59. Yang I-Y, Johnson R, Grollman AP, Moriya M. Genotoxic mechanism for the major acrolein-derived deoxyguanosine adduct in human cells. Chem. Res. Toxicol 2002;15:160–164. [PubMed: 11849041]
60. Sanchez AM, Minko IG, Kurtz AJ, Kanuri M, Moriya M, Lloyd RS. Comparative evaluation of the bioreactivity and mutagenic spectra of acrolein-derived α-HOPdG and γ-HOPdG regioisomeric deoxyguanosine adducts. Chem. Res. Toxicol 2003;16:1019–1028. [PubMed: 12924930]
61. VanderVeen LA, Hashim MF, Nechev LV, Harris TM, Harris CM, Marnett LJ. Evaluation of the mutagenic potential of the principal DNA adduct of acrolein. J. Biol. Chem 2001;276:9066–9070. [PubMed: 11106660]
62. Bessho T. Induction of DNA replication-mediated double strand breaks by psoralen DNA interstrand cross-links. J. Biol. Chem 2003;278:5250–5254. [PubMed: 12473662]
63. Kuraoka I, Kobertz WR, Ariza RR, Biggerstaff M, Essigmann JM, Wood RD. Repair of an interstrand DNA cross-link initiated by ERCC1-XPF repair/recombination nuclease. J. Biol. Chem 2000;275:26632–26636. [PubMed: 10882712]
64. Niedernhofer LJ, Odijk H, Budzowska M, van Drunen E, Maas A, Theil AF, de Wit J, Jaspers NG, Beverloo HB, Hoeijmakers JH, Kanaar R. The structure-specific endonuclease ERCC1-XPF is required to resolve DNA interstrand cross-link-induced double-strand breaks. Mol. Cell. Biol 2004;24:5776–5787. [PubMed: 15199134]
65. Zheng H, Wang X, Warren AJ, Legerski RJ, Nairn RS, Hamilton JW, Li L. Nucleotide excision repair- and polymerase η-mediated error-prone removal of mitomycin C interstrand cross-links. Mol. Cell. Biol 2003;23:754–761. [PubMed: 12509472]
66. Shen X, Jun S, O'Neal LE, Sonoda E, Bemark M, Sale JE, Li L. REV3 and REV1 play major roles in recombination-independent repair of DNA interstrand cross-links mediated by monoubiquitinated proliferating cell nuclear antigen (PCNA). J. Biol. Chem 2006;281:13869–13872. [PubMed: 16571727]
67. Sarkar S, Davies AA, Ulrich HD, McHugh PJ. DNA interstrand crosslink repair during G1 involves nucleotide excision repair and DNA polymerase ζ. Embo J 2006;25:1285–1294. [PubMed: 16482220]
68. Washington MT, Minko IG, Johnson RE, Wolfle WT, Harris TM, Lloyd RS, Prakash S, Prakash L. Efficient and error-free replication past a minor-groove DNA adduct by the sequential action of human DNA polymerases ι and κ. Mol. Cell. Biol 2004;24:5687–5693. [PubMed: 15199127]
69. Washington MT, Minko IG, Johnson RE, Haracska L, Harris TM, Lloyd RS, Prakash S, Prakash L. Efficient and error-free replication past a minor-groove N^2-guanine adduct by the sequential action of yeast Rev1 and DNA polymerase ζ. Mol. Cell. Biol 2004;24:6900–6906. [PubMed: 15282292]
70. Minko IG, Washington MT, Kanuri M, Prakash L, Prakash S, Lloyd RS. Translesion synthesis past acrolein-derived DNA adduct, γ - hydroxypropanodeoxyguanosine, by yeast and human DNA polymerase η. J. Biol. Chem 2003;278:784–790. [PubMed: 12401796]

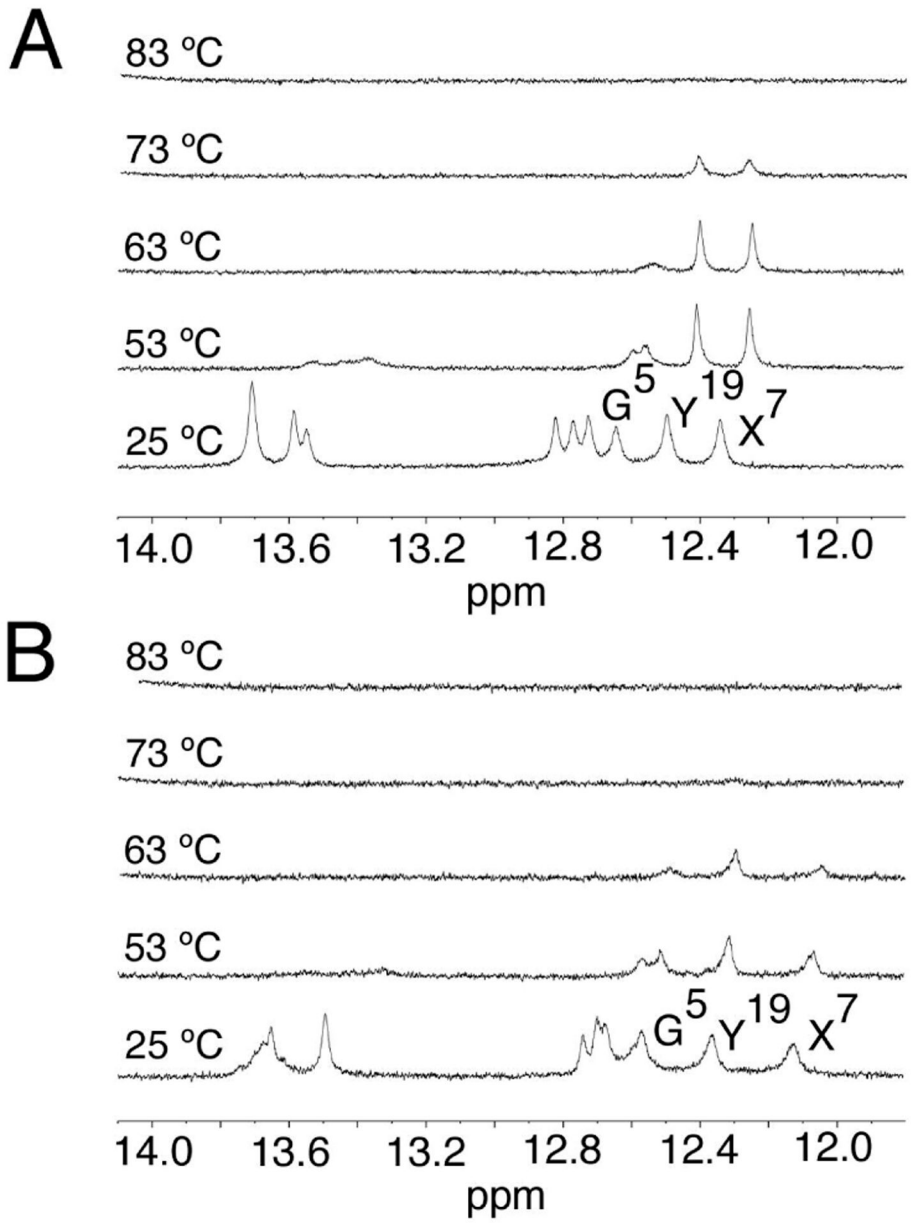

Figure 1. Expanded plots showing the imino proton region of the ^{1}H NMR spectrum as a function of temperature

A. The *R*-α-CH_3-γ-OH-1,N^2-propano-2′-deoxyguanosine cross-linked adduct. **B.** The *S*-α-CH_3-γ-OH-1,N^2-propano-2′-deoxyguanosine cross-linked adduct. The data were acquired at a ^{1}H frequency of 500 MHz.

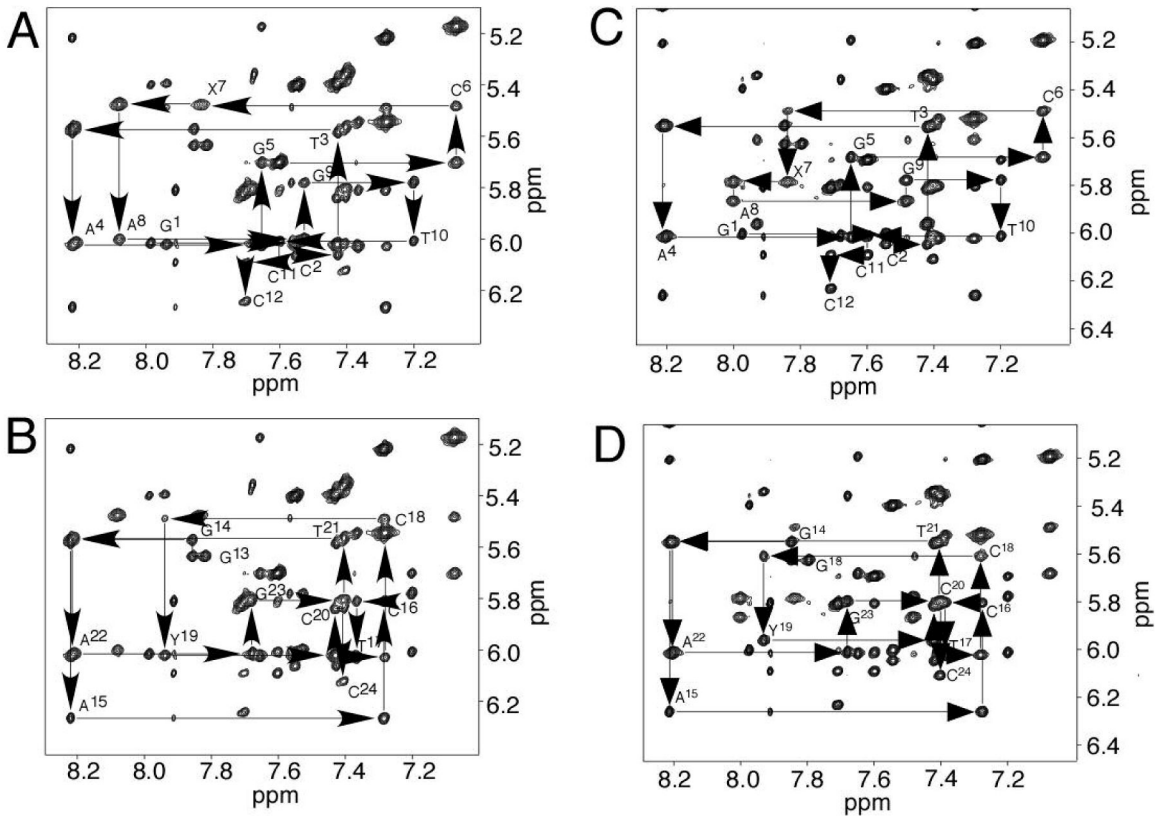

Figure 2. Expanded plots of ^{1}H NOESY spectra, showing sequential NOEs from the aromatic to the anomeric protons

A. The modified strand of the *R*-α-CH_3-γ-OH-1,N^2-propano-2′-deoxyguanosine cross-linked adduct. **B.** The complementary strand of the *R*-α-CH_3-γ-OH-1,N^2-propano-2′-deoxyguanosine cross-linked adduct. The NOE mixing time was 150 ms. **C.** The modified strand of the *S*-α-CH_3-γ-OH-1,N^2-propano-2′-deoxyguanosine cross-linked adduct. **D.** The complementary strand of the *S*-α-CH_3-γ-OH-1,N^2-propano-2′-deoxyguanosine cross-linked adduct. The NOE mixing time was 250 ms. For both the *R*- and *S*-cross-links, the data were acquired at a ^{1}H frequency of 800 MHz. The base positions are indicated at the intra-nucleotide cross-peaks of the aromatic protons to the anomeric protons.

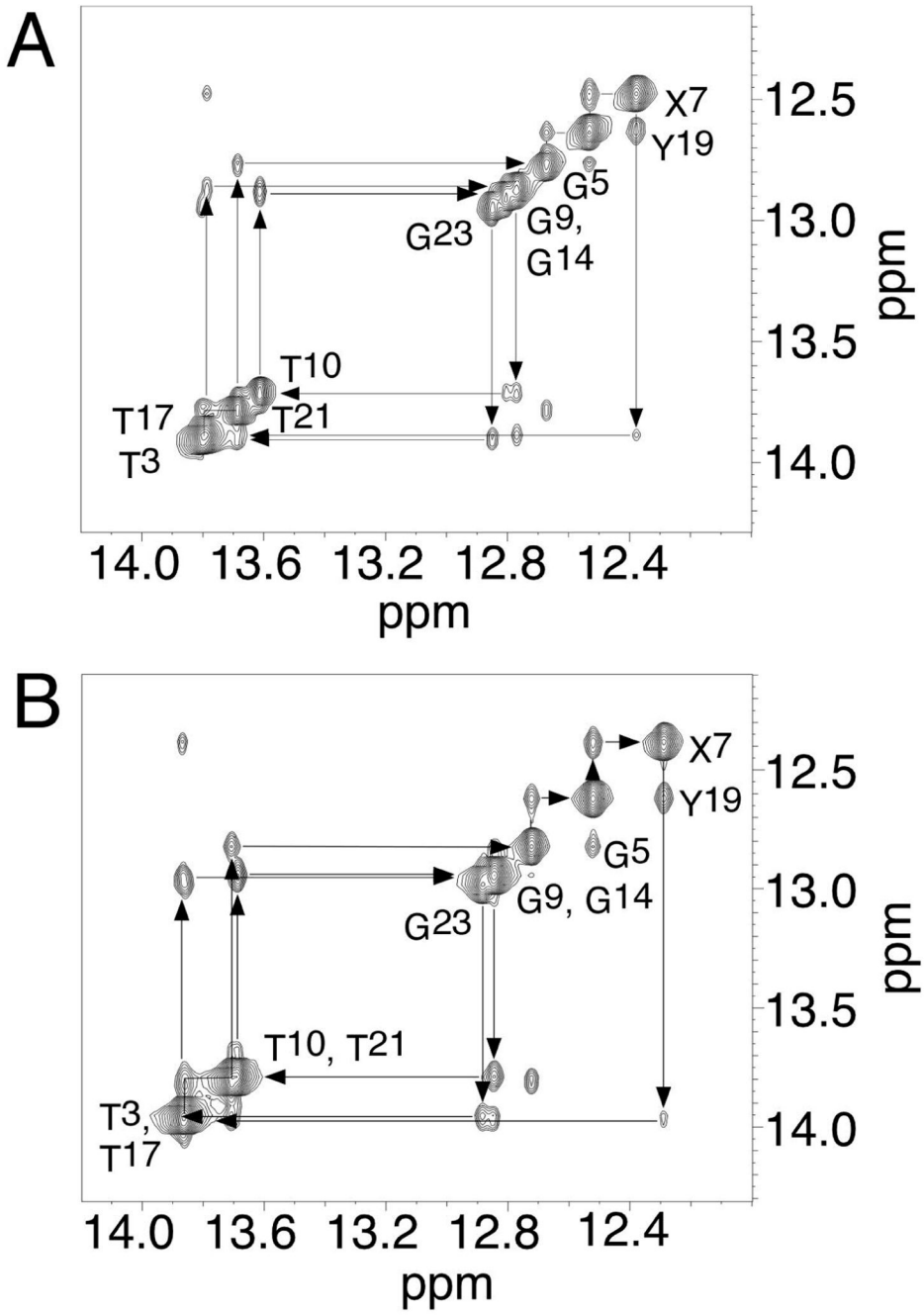

Figure 3. Expanded plots of NOESY spectra, showing sequential NOEs for the imino protons
A. The *R*-α-CH_3-γ-OH-1,N^2-propano-2′-deoxyguanosine cross-linked adduct. **B.** The *S*-α-CH_3-γ-OH-1,N^2-propano-2′-deoxyguanosine cross-linked adduct. The data were acquired at a ^{1}H frequency of 800 MHz, and a mixing time of 200 ms.

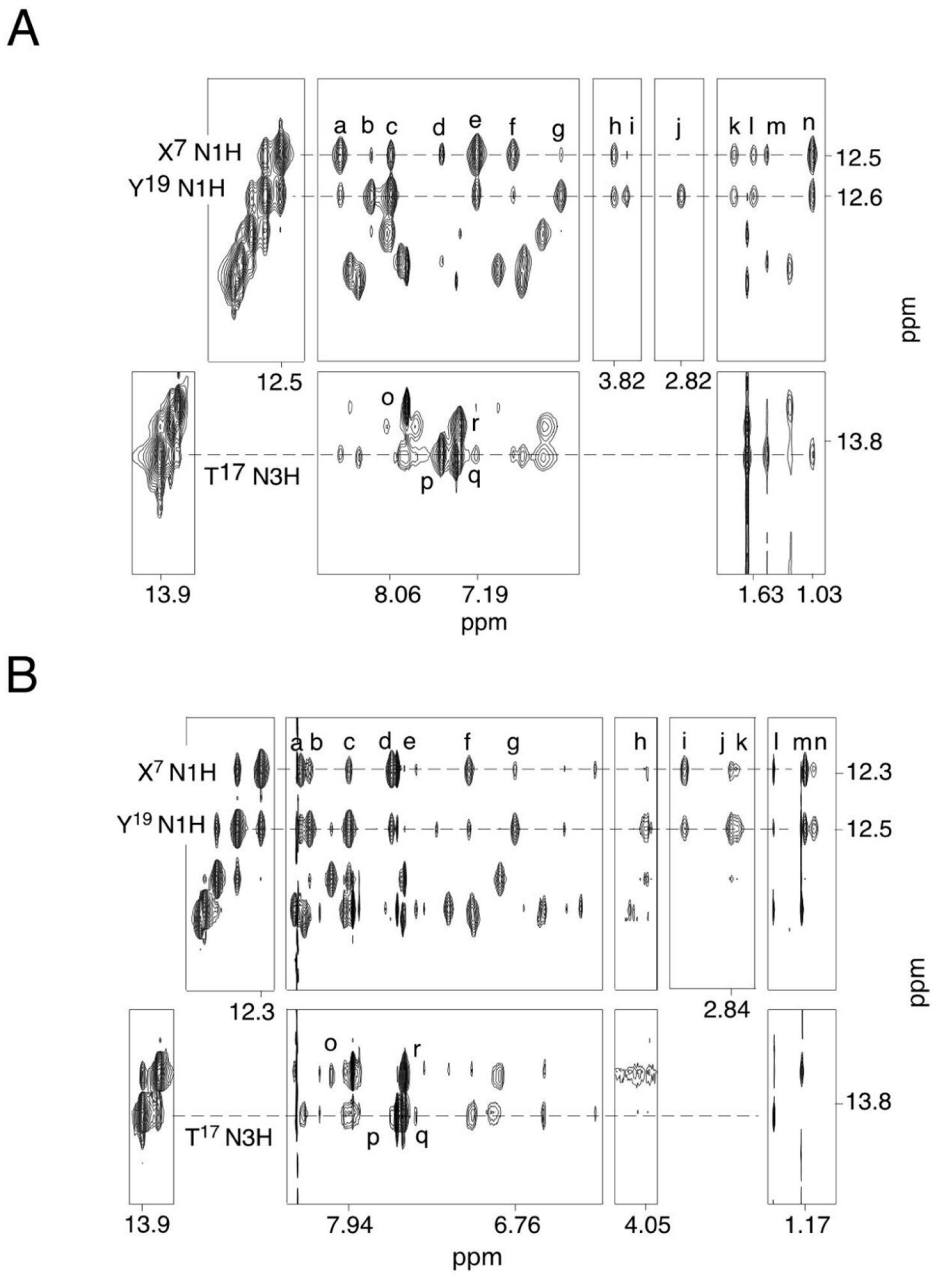

Figure 4.

A. The *R*-α-CH_3-γ-OH-1,N^2-propano-2′-deoxyguanosine cross-linked adduct. Tile plot of a NOESY spectrum showing dipolar couplings from selected imino protons to DNA protons. Crosspeak assignments a, C^{18} N^4H_a; b, C^6 N^4H_a; c, Y^{19} N^2H; d, A^8 H2; e, X^7 N^2H; f, C^{18} N^4H_b; g, C^6 N^4H_b; h, X^7 H_α; i, X^7 $H_{\gamma1}$; j, X^7 $H_{\gamma2}$; k, X^7 $H_{\beta1}$; l, X^7 $H_{\beta2}$; m, T^{17} CH_3; n, X^7 CH_3; o, A^{15} H2/T^{10} N3H; p, A^8 H2/T^{17} N3H; q, A^{22} H2/T^3 N3H; r, A^4 H2/T^{21} N3H. The data were acquired at a mixing time of 200 ms. **B.** The *S*-α-CH_3-γ-OH-1,N^2-propano-2′-deoxyguanosine cross-linked adduct. Tile plot of a NOESY spectrum showing dipolar coupling from selected imino protons to DNA protons. Crosspeak assignments a, C^{18} N^4H_a; b, C^6 N^4H_a; c, Y^{19} N^2H; d, X^7 N^2H; e, A^8 H2; f, C^{18} N^4H_b; g, C^6 N^4H_b; h, X^7 $H_{\gamma1}$; i, X^7 H_α; j, X^7

$H_{\gamma 2}$; k, X^{7} $H_{\beta 2}$; l, T^{17} CH_3; m, X^{7} CH_3; n, X^{7} $H_{\beta 1}$; o, A^{15} H2/T^{10} N3H; p, A^{8} H2/T^{17} N3H; q, A^{22} H2/T^{3} N3H; r, A^{4} H2/T^{21} N3H. The data were acquired at a mixing time of 250 ms.

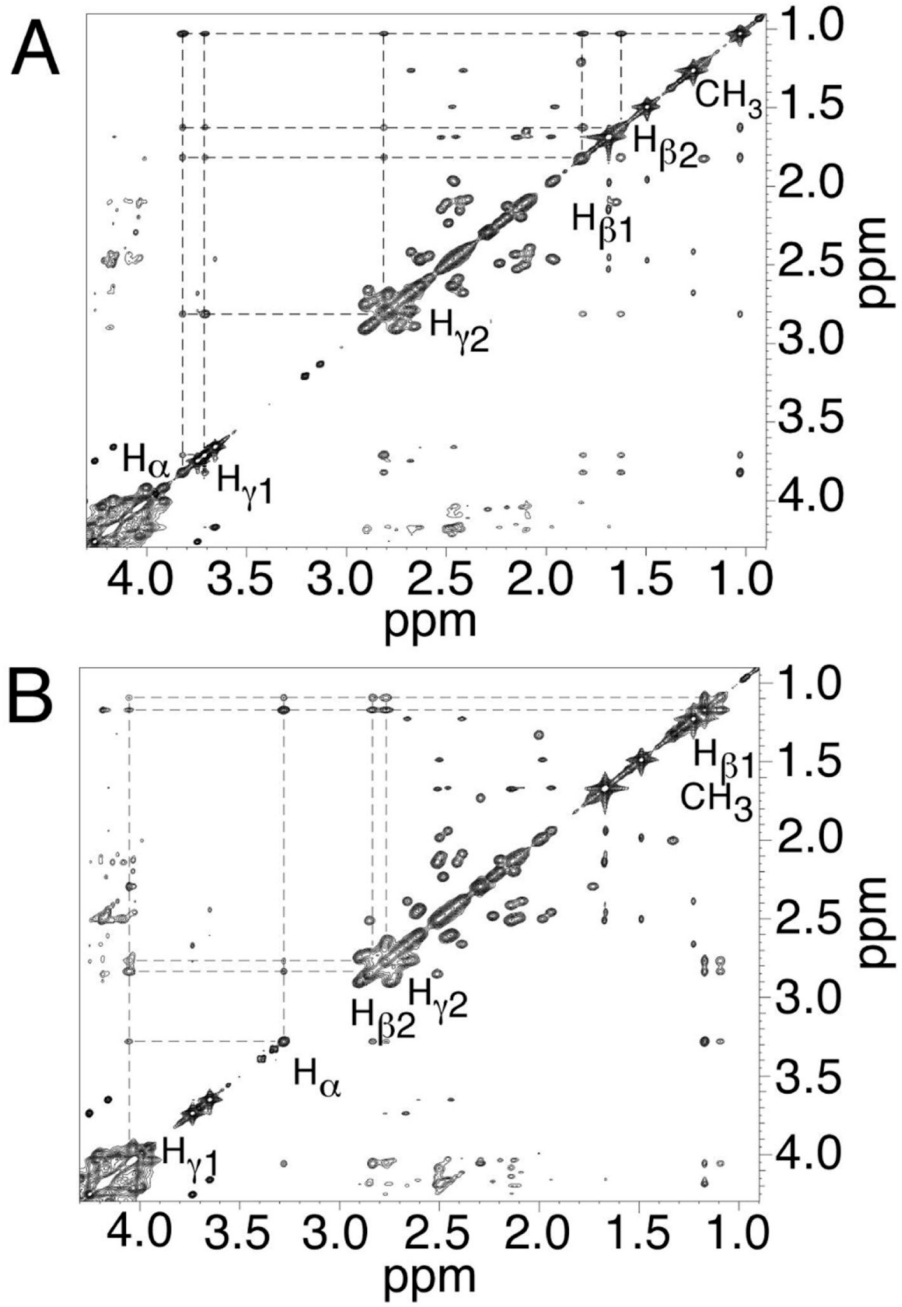

Figure 5. Expanded plots of ^{1}H NOESY spectra showing the assignments of the cross-linked protons
A. The *R*-α-CH_3-γ-OH-1,N^2-propano-2′-deoxyguanosine cross-linked adduct. **B.** The *S*-α-CH_3-γ-OH-1,N^2-propano-2′-deoxyguanosine cross-linked adduct. The data were acquired at a ^{1}H frequency of 800 MHz, and a mixing time of 200 ms.

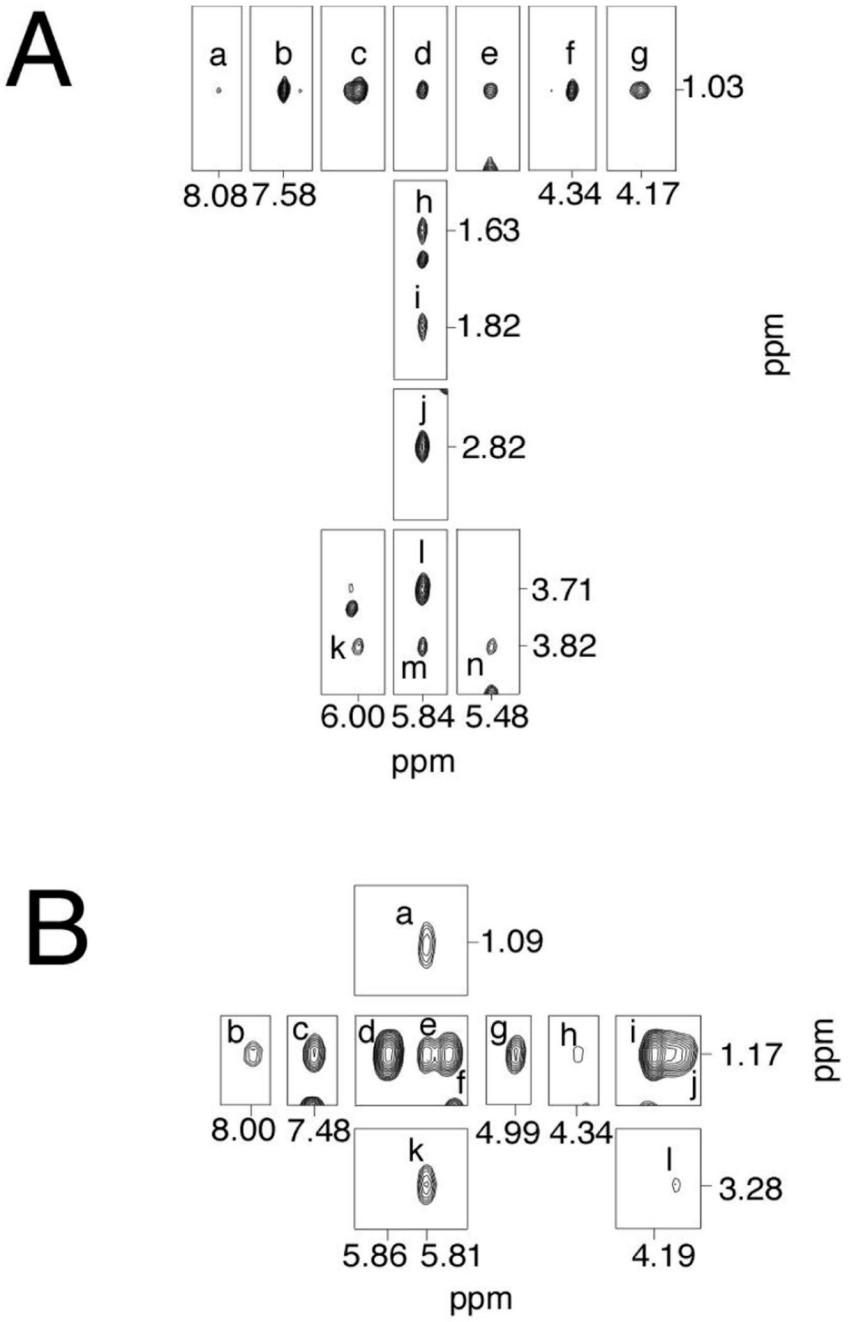

Figure 6. Tile plots showing NOEs between the cross-linked protons and DNA protons

A. The *R*-α-CH_3-γ-OH-1,N^2-propano-2′-deoxyguanosine cross-linked adduct. Crosspeaks a, A^8 H8→X^7 CH_3; b, A^8 H2→X^7 CH_3; c, A^8 H1′→ X^7 CH_3; d, C^{20} H1′→X^7 CH_3; e, X^7 H1′ →X^7 CH_3; f, A^8 H4′→X^7 CH_3; g, A^8 H5′→X^7 CH_3; h, C^{20} H1′→ X^7 $H_{\beta 2}$; i, C^{20} H1′→X^7 $H_{\beta 1}$; j, C^{20} H1′→ X^7 $H_{\gamma 2}$; k, A^8 H1′→X^7 H_α; l, C^{20} H1′→Y^{19} $H_{\gamma 1}$; m, C^{20} H1′→X^7 H_α; n, X^7 H1′→X^7 H_α. The mixing time was 350 ms. **B.** The *S*-α-CH_3-γ-OH-1,N^2-propano-2′-deoxyguanosine cross-linked adduct. Crosspeaks a, C^{20} H1′→X^7 $H_{\beta 1}$; b, A^8 H8 →X^7 CH_3; c, A^8 H2→X^7 CH_3; d, A^8 H1′→X^7 CH_3; e, C^{20} H1′→X^7 CH_3; f, X^7 H1′→X^7 CH_3; g, A^8 H3′ →X^7 CH_3; h, X^7 H4′→X^7 CH_3; i, A^8 H4′→X^7 CH_3; j, C^{20} H4′→ X^7 CH_3 (overlapped); k, C^{20} H1′→X^7 H_α; l, C^{20} H4′→X^7 H_α.

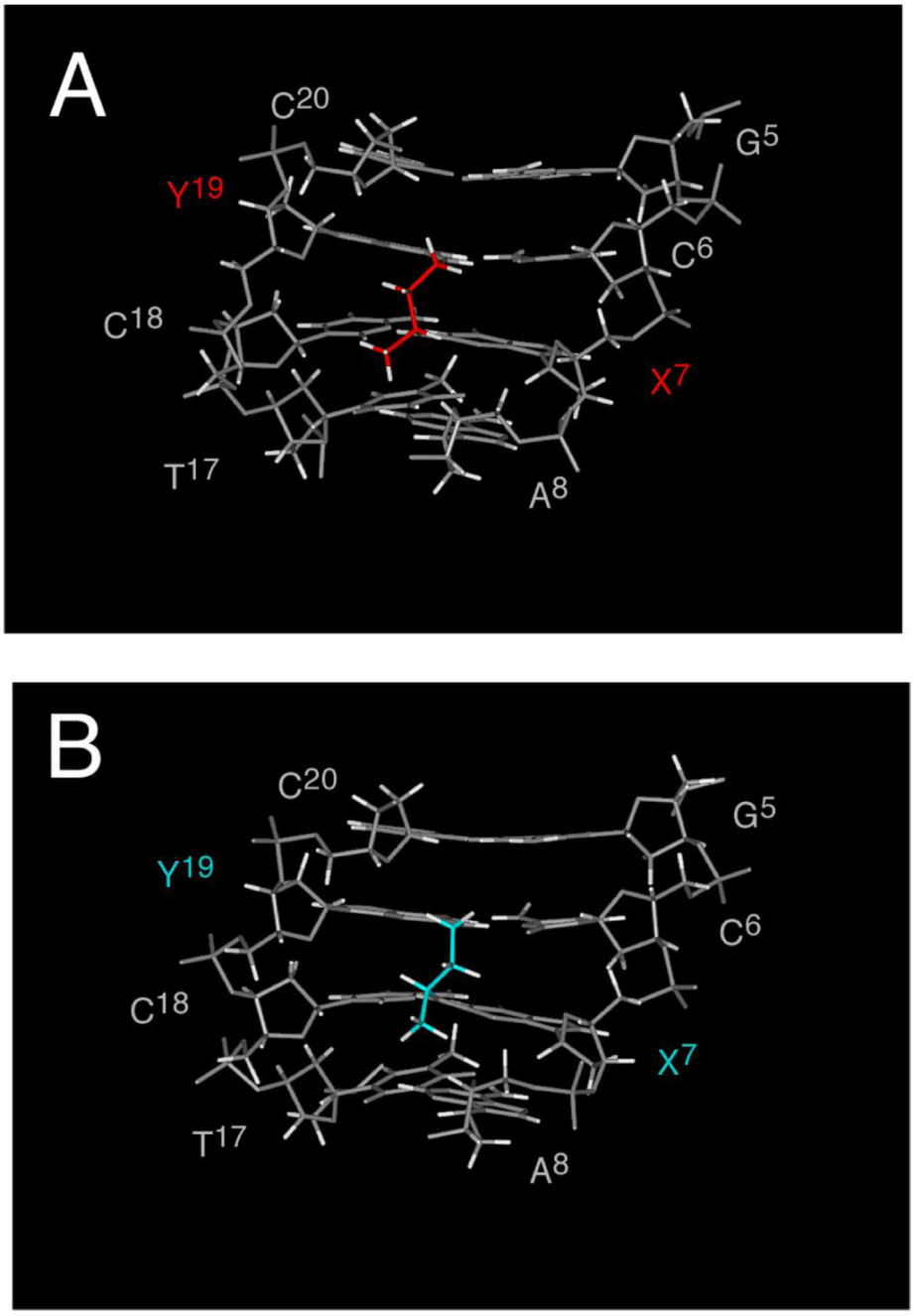

Figure 7. Views of the refined structures for the *R*- and *S*-crosslinked oligodeoxynucleotides, shown from the minor groove

A. The *R*-α-CH_3-γ-OH-1,N^2-propano-2′-deoxyguanosine cross-linked adduct (red). **B.** The *S*-α-CH_3-γ-OH-1,N^2-propano-2′-deoxyguanosine cross-linked adduct (blue).

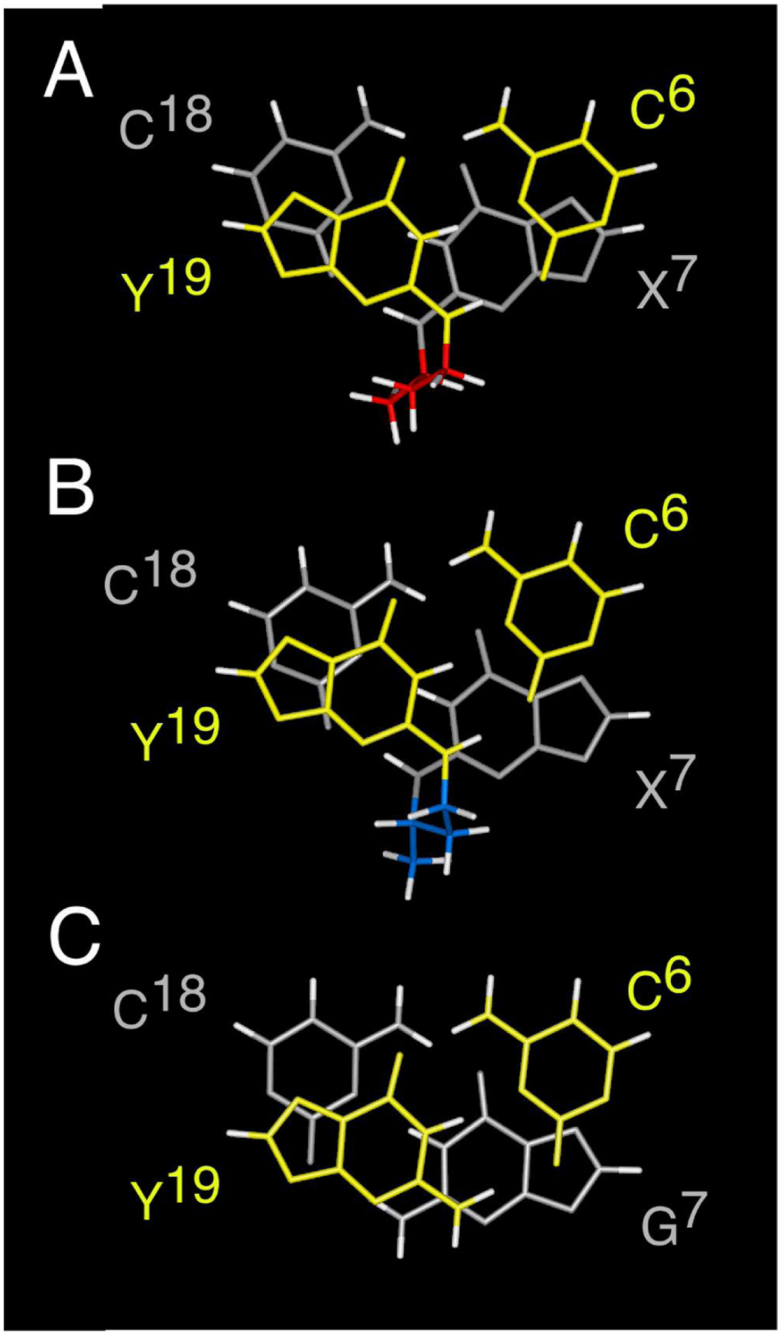

Figure 8.

A. Stacking of base pairs C^6•Y^{19} (yellow) and X^7•C^{18} (grey) for the *R*-α-CH_3-γ-OH-1,N^2-propano-2′-deoxyguanosine cross-linked adduct (red). **B.** Stacking of base pairs C^6•Y^{19} (yellow) and X^7•C^{18} (grey) for the *S*-α-CH_3-γ-OH-1,N^2-propano-2′-deoxyguanosine cross-linked adduct (blue). **C.** Stacking of base pairs C^6•G^{19} (yellow) and G^7•C^{18} (grey) for the non-cross-linked adduct.

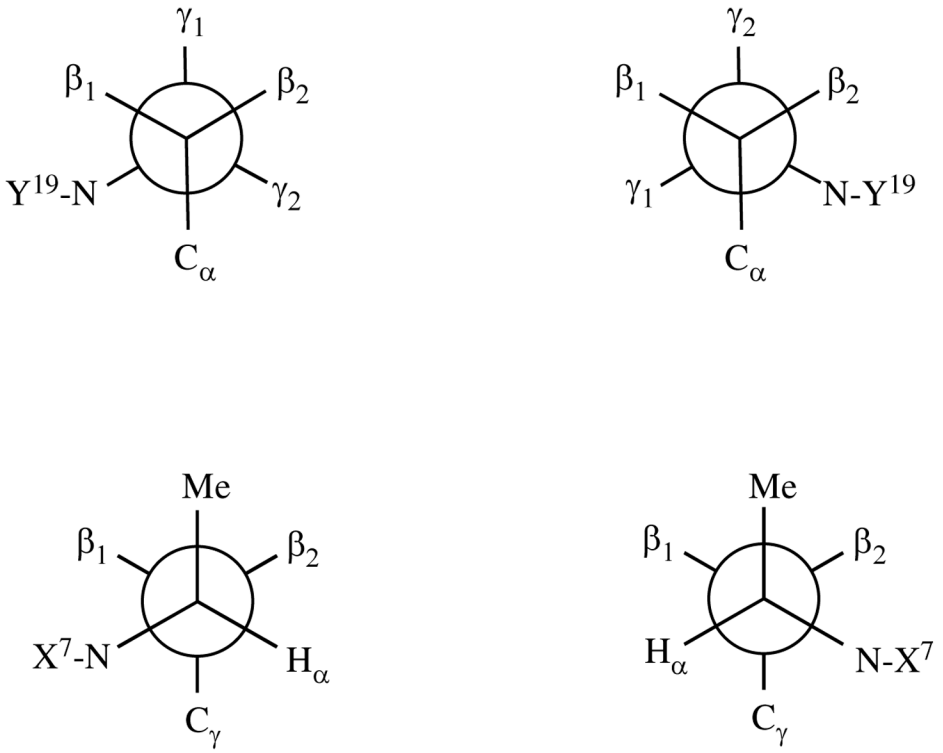

Figure 9.

A. Newman projections for the *R*-α-CH_3-γ-OH-1,N^2-propano-2′-deoxyguanosine cross-linked adduct. Top: View along the C_β-C_γ axis. Bottom: View along the C_α-C_β axis. **B.** Newman projections for the *S*-α-CH_3-γ-OH-1,N^2-propano-2′-deoxyguanosine cross-linked adduct. Top: View along the C_β-C_γ axis. Bottom: View along the C_α-C_β axis.

A

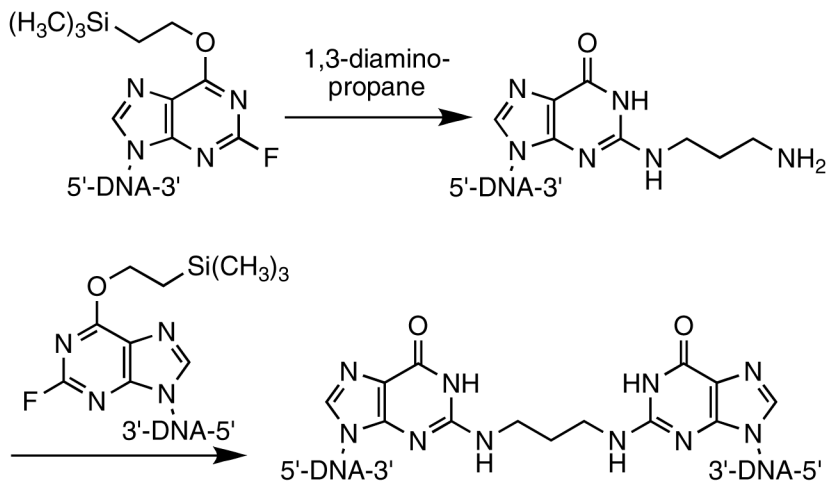

B

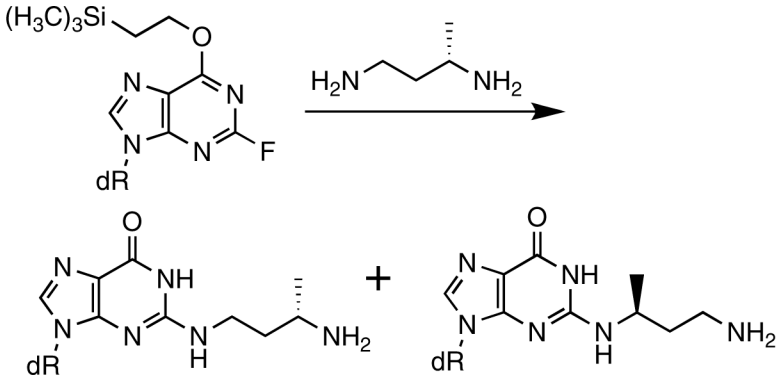

Scheme 1.

A. Synthesis of Trimethylene Inter-strand Cross-links of the Type N^2-dG-$(CH_2)_3$-N^2-dG (42).

B. The Nucleophilic Aromatic Substitution Reaction of (*S*)-1,3-Diaminobutane with Excess O^6-(2-Trimethylsilyl)-2-fluoroinosine Nucleoside.

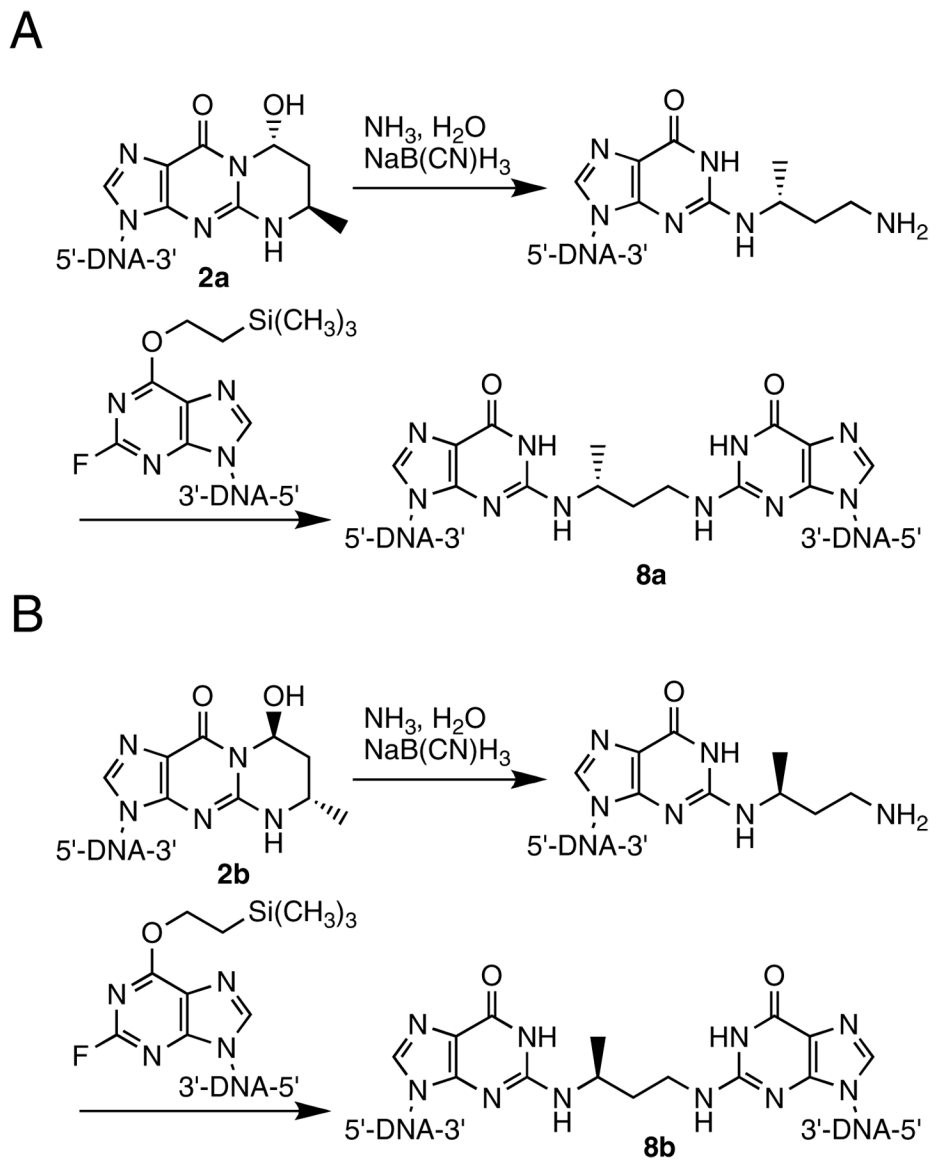

Scheme 2.

Synthesis of (**A**) the 5′-Cp-N^2-dG-3′-*R*-(α)-CH_3-Propyl-5′-Cp-N^2-dG-3′ and (**B**) the 5′-Cp-N^2-dG-3′-*S*-(α)-CH_3-Propyl-5′- Cp-N^2-dG-3′ Inter-strand DNA Cross-links **8a** and **8b** in the 5′-CpG-3′ Sequence.

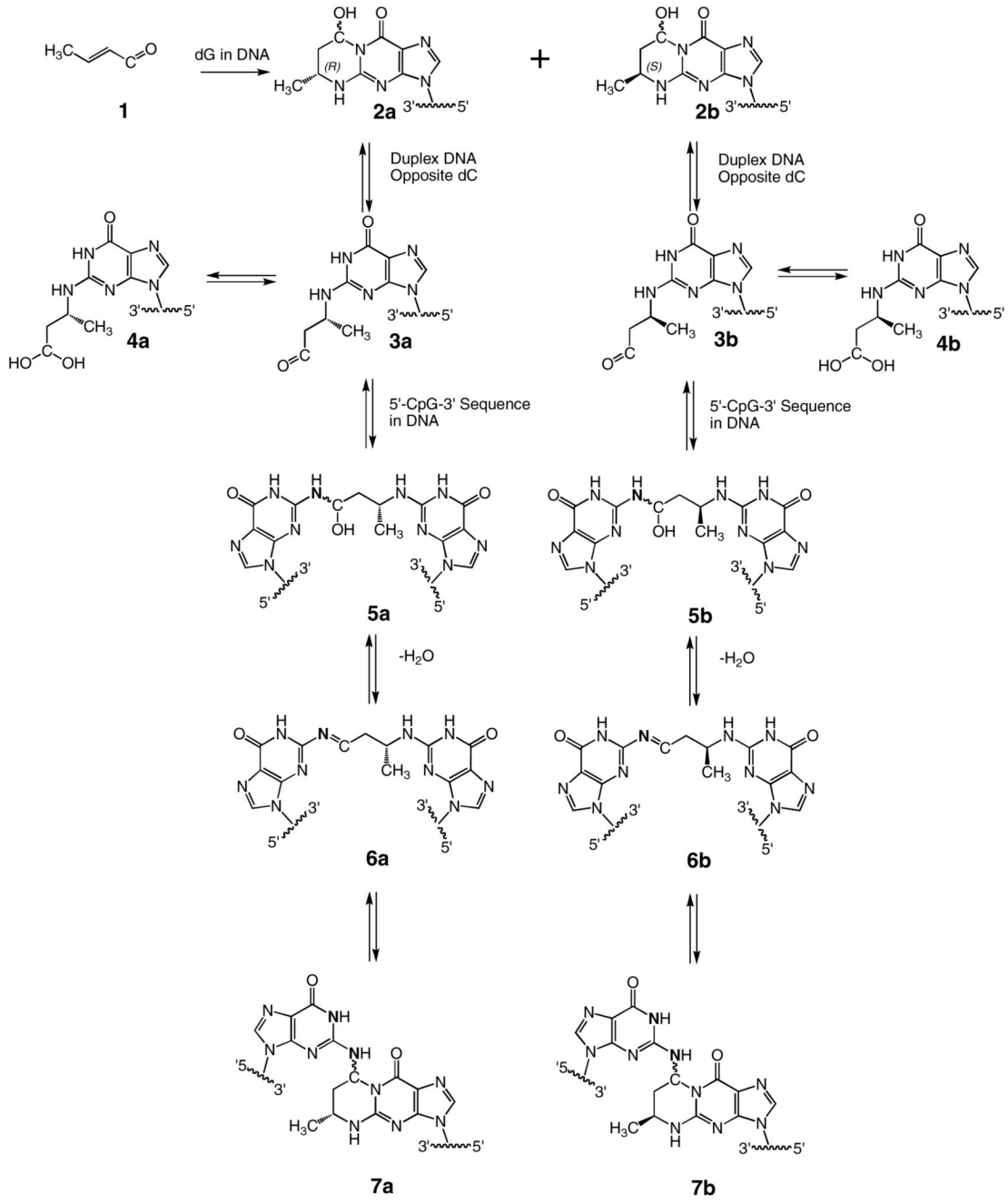

Chart 1.
Equilibrium Chemistry of the *R*- and *S*-α-CH_3-γ-OH-PdG Adducts in the 5′-CpG-3′ Sequence in Duplex DNA.

A

5′-G[1] C[2] T[3] A[4] G[5] C[6] **X[7]** A[8] G[9] T[10]C[11]C[12]-3′
3′-C[24]G[23]A[22]T[21]C[20]**Y[19]**C[18]T[17]C[16]A[15]G[14]G[13]-5′

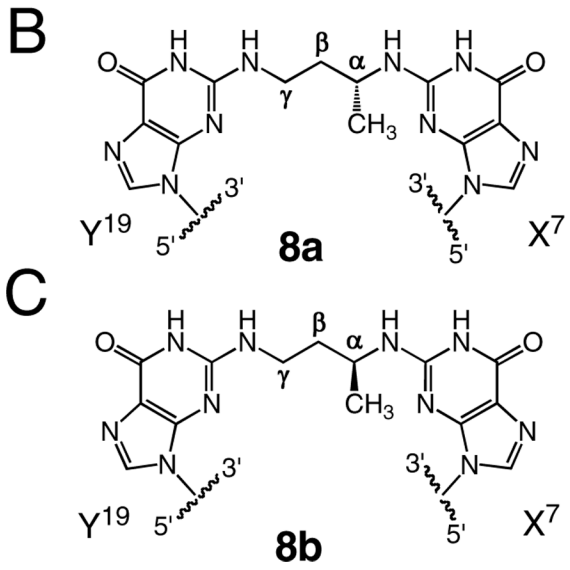

Chart 2.
A. The duplex oligodeoxynucleotide containing the 5′-CpG-3′ sequence. **B.** The reduced *R*-α-CH_3-γ-OH-1,N^2-propano-2′-deoxyguanosine cross-linked adduct **8a. C.** The reduced *S*-α-CH_3-γ-OH-1,N^2-propano-2′-deoxyguanosine cross-linked adduct **8b.**

Table 1

Chemical Shifts (ppm) of the 5′-Cp-N^2-dG-3′-*R*-(α)-CH_3-Propyl-5′-Cp-N^2-dG-3′ and 5′-Cp-N^2-dG-3′- *S*-(α)-CH_3-Propyl-5′-Cp-N^2-dG-3′ Inter-strand DNA Cross-links **8a** and **8b**.

	$X^7N^2H^a$	CH_3	H_α	$H_{\beta 1}$	$H_{\beta 2}$	$H_{\gamma 1}$	$H_{\gamma 2}$	$Y^{19}N^2H^a$
R-cross-link **8a**	7.19	1.03	3.82	1.82	1.63	3.71	2.82	8.06
S-cross-link **8b**	7.47	1.17	3.28	1.09	2.77	4.06	2.84	7.89

[a] chemical shift was measured in water at 13 °C.

Table 2

Structural Statistics for the 5′-Cp-N^2-dG-3′- *R*-(α)-CH_3-Propyl-5′- Cp-N^2-dG-3′ and 5′-Cp-N^2-dG-3′-*S*-(α)-CH_3-Propyl-5′- Cp-N^2-dG-3′ Inter-strand DNA Cross-links **8a** and **8b**.

NMR restraints	***R* crosslink 8a**	***S* crosslink 8b**
Total number of distance restraints	246	362
Interresidue distance restraints	119	161
Intraresidue distance restraints	127	201
DNA— adduct proton distance restraints	10	10
Adduct proton distance restraints	14	13
H-bonding restraints	52	52
pairwise rmsd (Å) over all atoms		
IniA vs. IniB	6.37	6.39
<rMDA>[a] vs. <rMDA>	0.53 ± 0.27	0.44 ± 0.23
<rMDB>[b] vs. <rMDB>	0.47 ± 0.24	0.26 ± 0.14
$rMDA_{avg}$[c] vs. $rMDB_{avg}$[d]	1.38	1.17
$rMDA_{avg}$ vs. rMD_{avg}[e]	0.80	0.77
$rMDB_{avg}$ vs.rMD_{avg}	1.01	0.74
IniA vs. rMD_{avg}	4.34	4.26
IniB vs. rMD_{avg}	2.62	2.50

[a] <rMDA> represents the set of 5 structures that emerged from rMD calculations starting from IniA.

[b] <rMDB> represents the set of 5 structures that emerged from rMD calculations starting from IniB.

[c] $rMDA_{avg}$ represents the average structure of all five <rMDA>.

[d] $rMDB_{avg}$ represents the average structure of all five <rMDB>.

[e] rMD_{avg} represents the potential energy minimized average structure of all 10 structures of <rMDA> and <rMDB>.